

Planetary Atmospheres: Chemistry & Composition

Channon Visscher

Dordt University, Sioux Center, Iowa 51250, USA

Space Science Institute, Boulder, Colorado, 80301, USA

channon.visscher@dordt.edu

November 2, 2021

Abstract

The observed composition of a planetary atmosphere is the product of planetary formation and evolution, including the chemical and physical processes shaping atmospheric abundances into the present day. In our solar system, the gas giant planets Jupiter, Saturn, Uranus, and Neptune possess massive molecular envelopes consisting mostly of H_2 and He along with various minor amounts of heavy elements such as C, N, and O (present as CH_4 , NH_3 , and H_2O , respectively) and numerous additional minor species. The terrestrial planets Venus, Earth, and Mars each possess a relatively thin atmospheric envelope surrounding a rocky surface. The atmospheres of Mars and Venus are characterized by abundant CO_2 with a small amount of N_2 , whereas the atmosphere of the Earth is dominated by N_2 and O_2 . Such differences provide clues to the divergent pathways of atmospheric evolution.

Numerous closely coupled physical and chemical processes give rise to the abundances observed in the planetary atmospheres of our solar system. These processes include the maintenance of thermochemical equilibrium, reaction kinetics, atmospheric transport, photochemistry, condensation (including cloud formation) and vaporization, deposition and sublimation, diurnal and seasonal effects, greenhouse effects, surface-atmosphere reactions, volcanic activity, and (in the case of Earth) biogenic and anthropogenic sources. Our present understanding of the chemical composition of planetary atmospheres is the result of over a century of observations, including ground-based, space-based, and *in-situ* measurements of the major, minor, trace, and isotopic species found on each planet. These observations have been accompanied by experimental studies of planetary materials and the development of theoretical models to identify the key processes shaping atmospheric abundances observed today.

Keywords: planetary atmosphere; ground-based; space observation; terrestrial planets; giant planets; chemical composition; troposphere; stratosphere; sources and sinks

1 Observations of planetary atmospheres before the era of spacecraft exploration

Our understanding of the composition and chemical processes of planetary atmospheres has paralleled the development of planetary science as a modern field of study. The earliest efforts at characterizing planetary environments were based upon a combination of descriptive telescopic observations (including those of Robert Hooke and Giovanni Cassini in the 1660s) accompanied by experiences of our own terrestrial atmosphere. By the late 18th century, the existence of atmospheres on other planets was demonstrated by Mikhail Lomonosov and Thorbern Bergman during the 1761 transit of Venus (e.g., see Marov 2004). Improving telescopic observations provided evidence of atmospheric processes akin to those on the Earth, such as found in William Herschel's description of seasonal cycles in the polar regions of Mars (e.g., Herschel 1784).

A number of key developments in chemical spectroscopy (e.g., see Thomas 1991) in the 19th century provided the methods first employed toward the detection and quantification of chemical species in planetary atmospheres. By 1814, Joseph von Fraunhofer had invented the modern version of the spectroscope, which was soon put to use to explore absorption features in light from the Sun and bright stars. Early spectroscopic observations of the planets were described by William Huggins and Angelo Secchi in the 1860s and 1870s, based upon visual observations of major spectral features at visible wavelengths (e.g., Huggins 1867; Dunham 1949) and by the 1870s the ongoing development of astro-photographic techniques led to the first spectrographs capable of recording planetary reflection spectra (e.g., Draper 1877, 1879; Huggins 1876). Meanwhile, the study of atomic and molecular spectroscopy had also continued to advance, led by the pioneering work of Kirchhoff and Bunsen (Kirchhoff 1860; Kirchhoff & Bunsen 1860) on visible and ultraviolet spectra, followed by the development of infrared spectroscopy. By the early 20th century, the characteristic absorption features of numerous molecules had been measured, paving the way for their chemical identification and quantification in the spectra of planetary atmospheres.

A snapshot of our understanding of planetary atmospheres by the mid-20th century was summarized in *The Atmospheres of the Earth and Planets*, a collection papers edited by Gerard Kuiper (Kuiper 1952). Although ground-based observations of the planets are hampered by telluric absorption features (mitigated by using spectral features Doppler-shifted by relative planetary motions, or by comparison against solar or lunar spectra; e.g., see Slipher 1904), by the mid-20th century the bulk composition of each planetary atmosphere had been approximated from spectroscopic observations along with measurements of other properties, such as planetary density. Moreover, measurements of atmospheric scale heights from stellar occultation observations (e.g., Fabry 1929; Baum & Code 1953) provided information about the mean molecular weight of planetary atmospheres, yielding additional constraints on chemical composition. At the dawn of the era of spacecraft exploration (marked by the 1962 flyby of Venus by *Mariner 2*, and in the outer solar system by the 1973 flyby of Jupiter by *Pioneer 10*), ground-based observations had been used to

detect atmospheric species on Venus (CO₂), Mars (CO₂, H₂O), Jupiter (H₂, CH₄, NH₃), Saturn (H₂, CH₄), Uranus (H₂, CH₄), and Neptune (H₂, CH₄). In addition to these discoveries, numerous species continued to be found and analyzed in the terrestrial atmosphere by various methods, including chemical analysis, infrared spectroscopy, mass spectroscopy, and gas chromatography.

The advent of the space age was revolutionary for our modern understanding of planetary atmospheres, providing closer and clearer planetary views via flybys or orbiters and (in some cases) *in-situ* measurements (often via gas chromatography and/or mass spectrometry) from landers, rovers, and atmospheric entry probes. This spacecraft exploration has been accompanied by ongoing improvements in ground-based observational data, a growing suite of instrumental methods, the increasing availability of experimental results that describe the properties and behavior of planetary materials, and the continuing development of our theoretical understanding of key chemical processes shaping the composition of the atmospheres in our solar system.

2 The diversity of atmospheres in the solar system

A diverse range of planetary and satellite atmospheres can be found across the solar system, from tenuous atmospheres of “airless” worlds to the massive fluid envelopes of the gas giants. For example, the tenuous atmospheres of satellites and planets such as the Moon and Mercury behave as surface-bound exospheres with typical surface pressures of $\sim 10^{-14}$ bar (Moon) up to $\sim 10^{-12}$ bar (Mercury), consisting of H, He, O, Ne, and Ar and metal atoms (such as Na, K, Ca, and Mg) supplied by the solar wind, micrometeorite bombardment, impact vaporization, and surface sputtering (e.g., Potter & Morgan 1985, 1986; Killen & Ip 1999; Killen *et al.* 2007; Wurz *et al.* 2007; Domingue *et al.* 2007; Vervack *et al.* 2010; Merkel *et al.* 2017). Jupiter’s moon Io has an SO₂-rich atmosphere supplied by volcanism and sublimation, with surface pressures up to $\sim 10^{-7}$ bar (McGrath *et al.* 2004; Lellouch 2005). The atmospheres of Pluto and Neptune’s moon Triton have surface pressures of $\sim 10^{-6}$ bar and consist of N₂ with minor amounts of CH₄ and CO, subject to vapour pressure equilibrium and seasonal exchange with surface ices (e.g., Yelle & McGrath 1996; Elliot *et al.* 1998; Yelle & Elliot 1997; Summers *et al.* 1997; Spencer *et al.* 1997; Lellouch *et al.* 2010; Zalucha & Cook 2019). Other icy satellites in the outer solar system have tenuous atmospheres (e.g., Europa, Ganymede, Callisto, Enceladus, Rhea, Dione) supplied by surface sputtering, the sublimation of surface ices, or plumes. In contrast, Saturn’s moon Titan has a substantial N₂-rich atmosphere with CH₄ and other hydrocarbons that may produce hazes and/or condense as liquids at the surface conditions of 94 K and 1.5 bar (see review in Hörst 2017). The terrestrial planets Venus, Earth, and Mars have significant, long-lived atmospheres surrounding rocky surfaces. The atmospheres of Venus and Mars are characterized by abundant CO₂ whereas the atmosphere of Earth is dominated by N₂ and O₂. The giant planets Jupiter, Saturn, Uranus, and Neptune possess massive, hydrogen-rich atmospheric envelopes, with minor amounts of heavy

elements (i.e., heavier than He) such as C, N, and O, present respectively as CH₄, NH₃, and H₂O, along with numerous additional species.

The range of planetary and satellite atmospheres observed in the solar system is a natural consequence of divergent formation and evolutionary scenarios. For example, the hydrogen-rich envelopes of the giant planets (Jupiter, Saturn, Uranus, Neptune) suggest that their atmospheres were mostly captured from the protoplanetary disk during their initial formation, while there was still enough H and He gas in the disk available for significant accretion (e.g., see Lissauer 1993; Lunine *et al.* 2004; Taylor *et al.* 2004; Chambers 2014). Given their resemblance to a “protosolar-composition” gas, these atmospheres have traditionally been labeled *primary atmospheres*. For the smaller terrestrial planets (Venus, Earth, Mars), the relative lack of H and He and very low noble gas abundances suggest that atmospheric volatiles initially accreted or captured during planetary formation have been lost to escape. These so-called *secondary atmospheres* appear to be the result of impact accretion and outgassing (primarily via volcanic activity) of volatile-rich material (e.g., see reviews in Atreya *et al.* 1989) and numerous other sources and sinks operating over long timescales. The present-day atmospheres thus represent a record of the major processes that have shaped planetary formation and evolution throughout the history of the solar system.

This review summarizes the atmospheric chemistry and composition of solar system planets that have significant atmospheres, considering first the terrestrial planets Venus, Earth, Mars, followed by the gas giant planets Jupiter, Saturn, Uranus, and Neptune. For each of these planets, measurements of the atmospheric abundances are provided, along with a brief discussion of the key chemical processes that shape atmospheric composition.

3 The physical properties of planetary atmospheres

The structure of a planetary atmosphere (including, for example, the temperature, pressure, or molecular number density as a function of altitude) defines the conditions for atmospheric chemistry, and is likewise shaped by atmospheric composition and chemical processes. It is thus useful to consider the relevant physical parameters (see properties listed in Table 1) and structural relationships (e.g., Chamberlain & Hunten 1989; Frederick 2008) that provide the context for chemical processes in planetary atmospheres.

131

132

Table 1: Physical Properties of Planetary Atmospheres

Parameter	Venus	Earth	Mars	Jupiter	Saturn	Uranus	Neptune
semi-major axis (AU)	0.723	$\equiv 1.000$	1.523	5.205	9.582	19.201	30.047
solar constant (W/m^2)	2602.0	1361.1	586.5	50.2	14.8	3.7	1.5
equilibrium temperature (K)	227	254	210	110	81	58	47
surface/reference temperature (K)	740	288	214	165.0	134.8	76.4	71.5
surface/reference pressure (bar)	95.6	1.013	0.00636	$\equiv 1.0$	$\equiv 1.0$	$\equiv 1.0$	$\equiv 1.0$
surface/reference gravity (m/s^2)	8.87	9.798	3.71	24.79	10.44	8.87	11.15
mean molecular mass (amu)	43.45	28.97	43.34	2.30	2.34	2.63	2.72
atmospheric scale height (km)	15.9	8.4	10.8	24.1	47.3	27.7	20.0
dry adiabatic lapse rate (K/km)	7.8	9.8	5.0	2.2	1.0	1.1	1.4
tropopause temperature (K)	214	216	140	104	85	54	52
tropopause pressure (mbar)	200	220	0.01	140	80	100	200

Mean molecular mass information calculated from atmospheric abundances; outer planet tropopause info from Chamberlain & Hunten (1989); Venus tropopause info from Limaye *et al.* (2018). The equilibrium temperature is a blackbody approximation that parameterises thermal balance with the solar energy absorbed by the planet; the surface/reference temperature also includes contributions from a greenhouse effect and/or a heat flux from the planetary interior.

For terrestrial planets, the surface pressure provides a measure of the total mass of the overlying atmosphere:

$$P = \frac{m_a g}{A} = \sigma_a g, \quad (1)$$

where P is the pressure (Pa), g is the surface gravity (m s^{-2}), A is the surface area of the planet (m^2), m_a is the total mass (kg), and σ_a is the column mass (kg m^{-2}) of the atmosphere. In general, all planetary atmospheres may be assumed to be in hydrostatic equilibrium. The decrease in pressure with altitude (as the mass of the overlying atmosphere decreases) can thus be expressed by

$$dP = -\rho g dz, \quad (2)$$

where P is the pressure (Pa), ρ is the density (kg m^{-3}), g is the gravity (m s^{-1}), and z is the altitude (m). Assuming molar quantities (e.g., $n = 1$ and $V = V_m$) in the ideal gas law ($PV = nRT$), the atmospheric density is defined by

$$\rho = \frac{\mu}{V} = \frac{\mu P}{RT}, \quad (3)$$

where μ is the mean molecular weight (kg mol^{-1}), V is volume (m^{-3}), P is the pressure (Pa), R is the gas constant ($8.314 \text{ J K}^{-1} \text{ mol}^{-1}$), and T is the temperature (K). Substitution of the ideal gas

144 law into the hydrostatic equation yields

$$dP = -\frac{\mu g}{RT} P dz. \quad (4)$$

145 Integrating from some reference pressure P_o at altitude $z = 0$ to some pressure P at altitude z gives
146 an expression that describes the variation of pressure as a function of altitude:

$$P = P_o e^{-z/H}, \quad (5)$$

147 where H is the *atmospheric scale height* defined by

$$H = \frac{RT}{\mu g}, \quad (6)$$

148 describing the altitude over which there is a $1/e$ decrease in the atmospheric pressure and density.
149 Comparative atmospheric scale heights are provided in Table 1. Variations in pressure and density
150 with altitude thus depend upon the gravity, the mean molecular weight of atmospheric species,
151 and the atmospheric temperature gradient. The change in temperature as a function of altitude is
152 known as the *lapse rate* (Γ , K m^{-1} or more commonly K km^{-1}):

$$\Gamma = -\frac{dT}{dz}. \quad (7)$$

153 A dry adiabatic lapse rate (i.e., the scenario where no condensation is occurring) can be approxi-
154 mated from combining a form of the first law of thermodynamics ($C_p dT = V dP$) with the hydro-
155 static and density expressions above ($dP = -\rho g dz$ and $\rho = \mu/V$) to give

$$C_p dT = -V \rho g dz = -\mu g dz \quad (8)$$

156 where C_p is the average molar heat capacity of the atmospheric gas ($\text{J K}^{-1} \text{mol}^{-1}$) based upon its
157 chemical composition. Combining this expression with the hydrostatic relation in equation (4) and
158 integrating from $P_o \rightarrow P$, and $T_o \rightarrow T$, the profile of an adiabatic troposphere is thus given by

$$P = P_o (T/T_o)^{C_p/R}, \quad (9)$$

159 where P_o and T_o refer to some reference point in the atmosphere (e.g., 288 K and 1 bar on Earth).
160 Taken together, equations (1)-(9) demonstrate the importance of the closely coupled relationships
161 between pressure and density, thermal structure, planetary gravity, and chemical composition.

162 The abundances of individual atmospheric gases are typically reported as a mole fraction or
163 volume mixing ratio, defined as the ratio of the partial pressure of some gas i (P_i) relative to the
164 total atmospheric pressure (P). Depending upon relative abundance, this value may be reported as

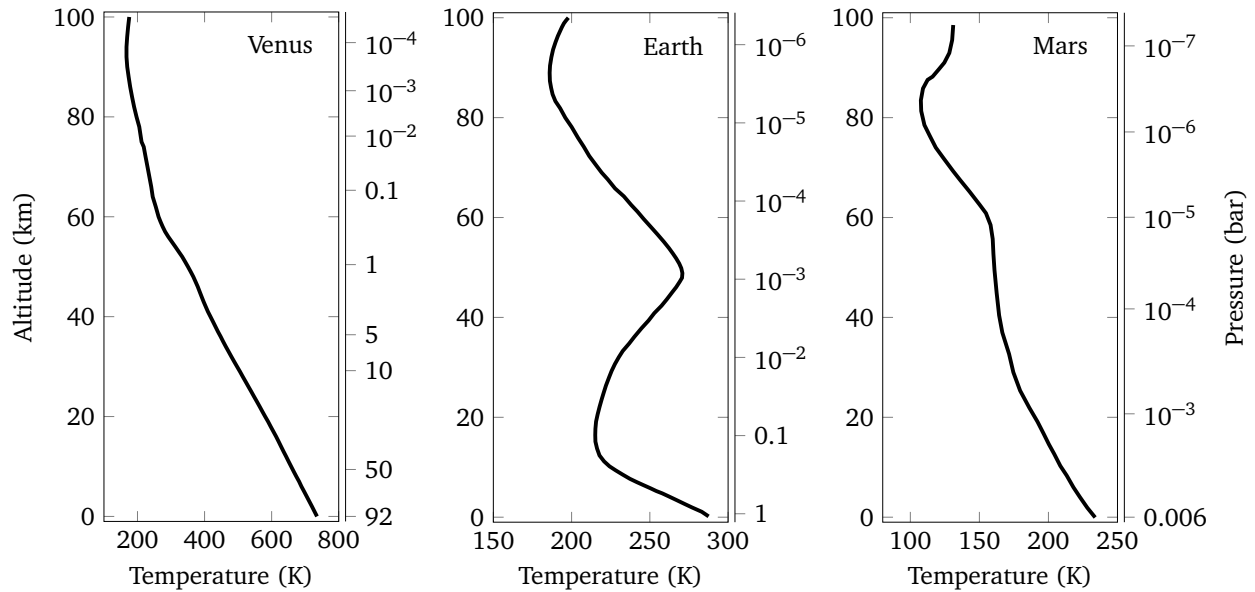


Figure 1: Atmospheric profiles for Venus, Earth, Mars from 0-100 km altitude (note different scales for temperature and pressure). Sources: U.S. Standard Atmosphere (NOAA/NASA/USAF 1976); Venus International Reference Atmosphere (VIRA; Seiff *et al.* 1985); Mars lander/rover entry data (e.g., Holstein-Rathlou *et al.* 2016; Schofield *et al.* 1997; Seiff & Kirk 1977)

percent (%), parts per million (ppm), parts per billion (ppb), or parts per trillion (ppt). The partial pressure can also be used with the ideal gas law ($n_i = P_i V / RT$) to determine the molar (e.g., mol cm^{-3}) or molecular (e.g., molecules cm^{-3}) number density of each atmospheric constituent.

4 Terrestrial planet atmospheres

The atmospheres of the terrestrial planets (Venus, Earth, and Mars) are relatively thin layers of gas surrounding rocky planetary surfaces. For example, over 99% of the mass of the Earth's atmosphere resides below an altitude of 40 km, compared to a mean planetary radius of 6371 km. The atmospheric profiles of Venus, Earth, and Mars to an altitude of 100 km are shown in Figure 1. These profiles are derived from the Venus International Reference Atmosphere (VIRA; Seiff *et al.* 1985) based upon the *Pioneer Venus* orbiter and atmospheric probes and the *Venera* 10, 12, and 13 descent craft for Venus; the U.S. Standard Atmosphere for the Earth (NOAA/NASA/USAF 1976); and atmospheric entry data derived from the *Mars Science Laboratory* (Holstein-Rathlou *et al.* 2016), *Mars Pathfinder* (Schofield *et al.* 1997), and the *Viking* landers Seiff & Kirk (1977) for Mars.

The atmospheric mass ratios and abundances of selected volatiles on the terrestrial planets (expressed as gram per gram of object) are summarized in Figure 2. The terrestrial planet atmospheres observed today appear to be secondary atmospheres mainly produced by the release of volatiles during impact accretion and subsequent out-gassing via volcanic activity. However, numerous

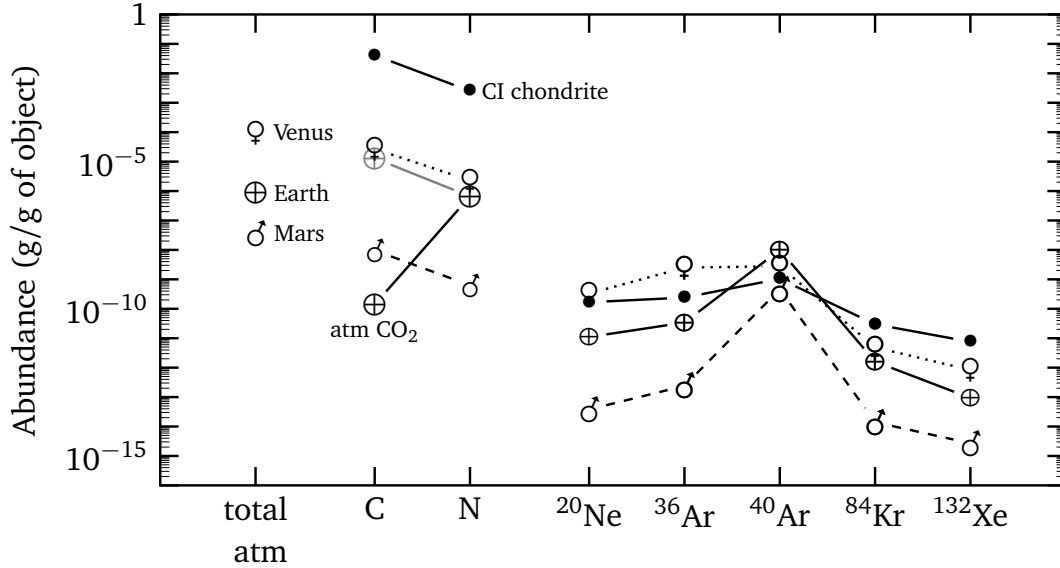


Figure 2: After Pepin (1991, 2006) and Pollack & Black (1982) using CI chondrite abundances from Lodders (2020) with the CI chondrite $^{40}\text{Ar}/^{36}\text{Ar}$ abundance ratio estimated from Mazor *et al.* (1970). Planetary atmosphere (g/g) abundances calculated from Tables 2-4 using isotope ratios from Pollack & Black (1982) along with measurements summarized in Fegley (2014) for Venus and reported by Mahaffy *et al.* (2013) for Mars. The abundance of atmospheric carbon as CO_2 is 10^{-10} g/g for the Earth whereas, the total carbon inventory in the Earth’s lithosphere (indicated in grey) corresponds to $\sim 10^{-5}$ g/g.

source and sink processes have shaped terrestrial atmospheric compositions throughout the history of the solar system, including capture from the protoplanetary disk, impact accretion, volcanic outgassing, impact erosion, stripping from the solar wind, atmospheric escape, surface-atmospheric interactions, exchange with interior reservoirs, metamorphism, weathering, and biological activity.

The relative lack of any remnant primordial atmosphere is implied by the behavior of the abundant light gases H_2 and He and the very low atmospheric concentrations of the nonradiogenic noble gases (cf. Trieloff 2017). For example, H_2 and He are expected to comprise a significant component of any atmosphere initially captured from the protoplanetary disk, but these light gases are readily lost from the low-gravity environments of the terrestrial planets. However, the production of a secondary atmosphere is not simply the loss of some initial H_2 and He inventory, as the heavier (and thus less subject to thermal escape) noble gases Ne, Ar, Kr, and Xe are also present at abundances much lower than expected for a primordial (or protosolar-composition) atmosphere. The presence of a secondary atmosphere is further supported by the relatively high abundance of radiogenic or “outgassed” noble gas isotopes such as ^{40}Ar , produced from the radioactive decay of accreted ^{40}K . Modern studies have continued to explore how these volatile element and isotopic abundance patterns provide clues about the origin and evolution of terrestrial planet atmospheres (e.g., see Atreya *et al.* 1989; Pepin 1991; Marty 2012; Halliday 2013; Avicé & Marty 2020; Lam-

mer *et al.* 2021, and references therein)

4.1 Venus

The atmosphere of Venus is notable for its high surface temperature and pressure (740 K and 95.6 bar at the modal radius of 6051.4 km), and consists of 96.5% CO₂ with 3.5% N₂ along with smaller amounts of SO₂, H₂O, CO, OCS, the noble gases, and other reactive species. The composition of the lower atmosphere of Venus is summarized in Table 2.

Table 2: Composition of the lower atmosphere of Venus

Gas	Abundance	Source	Sink
CO ₂	96.5%	volcanic outgassing; carbonates	photochemistry;
N ₂	3.5%	volcanic outgassing	NO _x formation by lightning
SO ₂ [†]	150 ppm	volcanic outgassing; S oxidation	H ₂ SO ₄ clouds; sulfates, sulfides
³⁶ Ar	31 ppm	volcanic outgassing; primordial	none
⁴⁰ Ar	30 ppm	volcanic outgassing; ⁴⁰ K decay	none
H ₂ O [†]	30 ppm	volcanic outgassing	H escape; oxidation of Fe ⁺²
CO [†]	17 ppm	CO ₂ photolysis	photooxidation; OCS formation
He	9 ppm	volcanic outgassing	escape
Ne	7 ppm	volcanic outgassing; primordial	none
OCS [†]	4.4 ppm	volcanic outgassing; CO sulfurization	conversion to SO ₂ ; S-bearing minerals
H ₂ S [†]	3 ppm	volcanic outgassing	conversion to SO ₂ ; S-bearing minerals
HCl	0.4 ppm	volcanic outgassing	Cl-bearing mineral formation
SO [†]	20 ppb	photolysis of SO ₂	photolysis; oxidation
S ₁₋₈ [†]	20 ppb	polysulfur cycle; surface reactions	conversion to SO ₂
Kr	~25 ppb ^a	volcanic outgassing; primordial	none
H ₂ SO ₄ [†]	4-10 ppm	oxidation of S-bearing gases	cloud formation; dehydration to SO ₃
Xe	~7 ppb ^a	volcanic outgassing; primordial	none
HF	5 ppb	volcanic outgassing	F-bearing mineral formation

Table adapted after abundances and sources/sinks compiled in Lodders & Fegley (1998) and Fegley (2014); cf. von Zahn *et al.* (1983); Moroz & Zasova (1997); Bézard & de Bergh (2007); Zolotov (2019); Vandaele (2020). ^aModel-dependent estimate; [†]Abundances are altitude-dependent and the abundance measurement at the lowest available altitude is listed here; see von Zahn *et al.* (1983); Fegley (2014); Marcq *et al.* (2018); Vandaele (2020) for details.

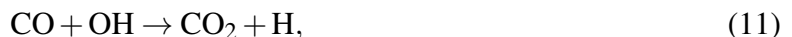
In the 1930s, the spectroscopic detection of large quantities of carbon dioxide in Venus' atmosphere (Adams & Dunham 1932; Adel & Slipher 1934) led Rupert Wildt to predict surface temperatures higher than the boiling point of water (Wildt 1940). This prediction was later confirmed by ground-based and *Mariner 2* microwave observations of Venus' thermal emission (Lilley 1961; Barath *et al.* 1964). The high surface temperatures are maintained by an intense greenhouse

effect. A bright and thick global layer of sulfuric acid clouds (measured by the *Pioneer Venus* large probe to be distributed between altitudes of 48-65 km) absorbs and reflects incident sunlight so effectively that the average incoming visible flux reaching the surface is significantly lower than that for the Earth: less than 4% of the incident shortwave flux at the top of the Venus' atmosphere is absorbed at Venus' surface (e.g., see Read *et al.* 2016). However, infrared emission from the surface and the sub-cloud atmosphere is very effectively absorbed by abundant CO₂ (~92 bar) along with SO₂ and other greenhouse gases.

In general, the observed chemical composition of Venus' atmosphere is a reflection of volcanic outgassing, high surface and crustal temperatures, and surface-atmosphere interactions. From a chemical standpoint it is convenient to divide the atmosphere into the region above the clouds, where UV-driven photochemistry dominates, and the sub-cloud region, where thermochemistry dominates. Photochemical models have thus played an important role in our understanding the chemistry of the upper atmosphere (e.g., see Yung & Demore 1982; Yung & DeMore 1999), and recent models also explore the role of thermochemical equilibria and diffusive atmospheric mixing (e.g., Krasnopolsky 2006, 2012; Bierson & Zhang 2020). Near the cloud layers and above, CO₂ in Venus' atmosphere is readily destroyed by photolysis:



The reverse reaction $\text{CO} + \text{O} \xrightarrow{\text{M}} \text{CO}_2$ is spin forbidden and therefore slow, and recombination of O is more likely to result in O₂. Without an efficient production route, CO₂ would thus be completely removed from Venus' atmosphere in about 5 million years. Moreover, a reaction important for Mars and Earth,

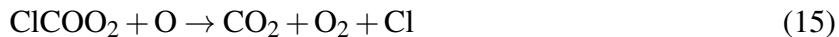


is not effective given insufficient OH production from H₂O, which is relatively scarce on Venus. Instead, a number of plausible catalytic reformation pathways have been proposed to resolve this stability problem, involving SO_x, NO_x, and/or ClO_x species. For example, Prinn (1971) first pointed out the potential importance of ClO_x for catalysing CO₂ formation on Venus. Near the cloud tops, atomic Cl is produced by the photolysis of HCl:

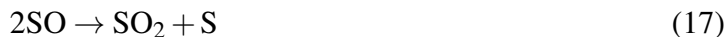


which readily reacts with CO to initiate a catalytic cycle that can efficiently recycle CO back into

CO₂:



Likewise, sulfur oxides (SO_x) are readily photolyzed and serve as a source of atomic O in the cycle (e.g., Winick & Stewart 1980; Yung & Demore 1982; Yung & DeMore 1999):



The above schemes can be combined in a larger cycle that results in the recycling of CO₂ and the formation of sulfuric acid via the series of reactions:



The identification of the cloud composition as sulfuric acid was proposed by Sill (1972) and Young (1973) based upon the spectral properties and refractive index of the cloud layers, along with the need for a desiccating agent that could remove H₂O. A sulfuric acid composition could also explain the apparent lack of SO₂, which was not detected until 1979 by ground-based UV observations (Barker 1979). At higher temperatures below the cloud base (48 km), sulfuric acid thermally decomposes via the reaction:

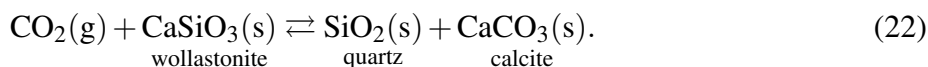


consistent with radio occultation observations that show a drop off in the H₂SO₄ vapour abundance below 48 km (Kolodner & Steffes 1998; Bézard & de Bergh 2007).

The high temperatures and obscuring cloud layers have made the lower atmosphere difficult to

observe. A handful of *in-situ* measurements (via gas chromatography and/or mass spectroscopy) of the lower atmosphere were made by the *Pioneer-Venus* probes, the *Venera 11-12* descent craft, and the *Venera 13-14* and *Vega 1-2* landers. However, on the *Pioneer-Venus* large probe the leak inlet for the mass spectrometer was apparently blocked by a cloud droplet from 50-30 km and possible insulation failure caused instruments to fail at 12.5 km, whereas the *Venera* and *Vega* landers did not return gas chromatograph data from below 12 km. More recently, night-side thermal emission in an infrared spectra window (in between CO₂ lines near 1 μ m), first detected by Allen & Crawford (1984), has allowed for additional measurements in the lower atmosphere below the clouds (e.g, see Marcq *et al.* 2006; Bézard & de Bergh 2007; Arney *et al.* 2014). However, the chemical abundances of the near-surface atmosphere remain uncertain, particularly for species that demonstrate altitude dependence. Theoretical modeling has thus served as an important tool for understanding chemical processes in this region of the atmosphere.

Given the high temperatures and pressures and the lack of ultraviolet flux, chemistry in the lower atmosphere is dominated by thermally-driven reactions and over long timescales may also be subject to gas-solid reactions at the surface, since 50% of the atmospheric mass resides below the 11-km summit of Maxwell Montes. A comprehensive exploration of chemical weathering and atmosphere-surface interactions can be found in Zolotov (2019); the salient points of interest for atmospheric composition are considered here. Of particular interest is the possibility that chemical equilibria of mineral phase assemblages found in the crust may regulate or “buffer” the abundance of key gases in the atmosphere. Among such reactions is that proposed by Harold Urey and Robert Mueller (Urey 1951; Mueller 1963, 1964):



If all three phases are present at equilibrium at a temperature of 740 K, this reaction yields a partial pressure of $P_{\text{CO}_2} \sim 90$, roughly similar to the observed partial pressure of CO₂ near the surface. However, the operation of this buffer depends upon whether carbonates are present on the surface of Venus, which remains a subject of debate, and CaCO₃ is unstable toward reaction with atmospheric SO₂ at Venus surface conditions. Most of the surface carbon inventory on Earth is found in crustal rocks as carbonates, whereas the carbon inventory of Venus - lacking a comparable carbon cycle - appears to be mostly present in the atmosphere (see Figure 2). This difference in carbon reservoirs is generally ascribed to the very dry conditions on Venus, and the high D/H ratio in Venus’ atmosphere (150 \times that of the Earth) suggests significant loss of water in the past.

The abundances of the volcanically-outgassed S-bearing species SO₂, OCS, H₂S, and S_x are altitude-dependent, shaped by photochemistry, atmospheric transport, thermally-driven reactions, and surface-atmosphere interactions as part of sulfur oxidation and polysulfur cycles (e.g., see Mills *et al.* 2007; Zhang *et al.* 2012; Marcq *et al.* 2018; Mills *et al.* 2019; Bierson & Zhang 2020;

Vandaele 2020). In the sulfur oxidation cycle, for example, the upward transport and oxidation of SO₂ and OCS leads to H₂SO₄ cloud formation. As these cloud droplets descend and evaporate, the SO₃ produced by the thermal decomposition of H₂SO₄ (Reaction 21) can recycle SO₂ and CO₂ via net reactions such as



In the polysulfur cycle, the upward transport and photodissociation of SO₂ and OCS produces S atoms, which can react with OCS to produce S₂:



Additional thermochemical reactions involving sulfur can produce higher sulfur allotropes S_n

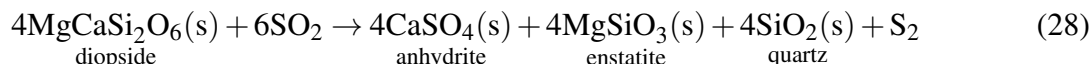
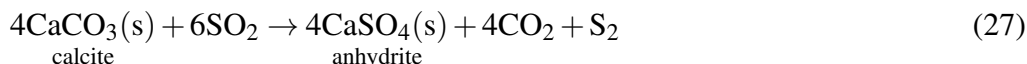


which have been proposed as a source of UV absorption in the upper atmosphere (Yung & DeMore 1999; Mills *et al.* 2007; Titov *et al.* 2018). Atmosphere-surface interactions may also serve as a source for sulfur species via reactions such as



consistent with the increase in abundance of OCS with decreasing altitude (Marcq *et al.* 2006; Bézard & de Bergh 2007; Fegley 2014).

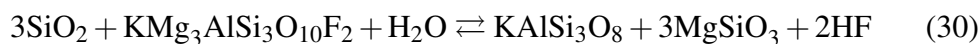
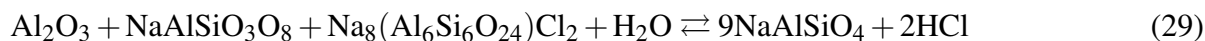
Sulfur dioxide, first detected in the UV spectrum of Venus (Barker 1979; Conway *et al.* 1979; Stewart *et al.* 1979), is the most abundant S-bearing gas and the third-most abundant gas Venus' atmosphere, and plays an important role in the catalytic recycling of CO₂ and sulfuric acid cloud formation. The atmospheric abundance of SO₂ is also high enough to drive surface-atmosphere reactions with carbonates (showing that CaCO₃ is unstable at present Venus surface conditions) and other Ca-bearing minerals via reactions such as



which serve as an atmospheric sink for SO₂. Such sulfurization reactions can thus be used to estimate the amount of volcanic outgassing necessary to maintain the observed SO₂ abundance (Fegley & Prinn 1989), and also serve as a proxy for the chemical weathering of surface rocks (Zolotov (2018)).

Other volcanic gases such as HCl and HF have also been detected in Venus' atmosphere

(Connes *et al.* 1967). As shown above, HCl photolysis is a source of Cl radicals in ClO_x catalytic cycles that produce CO_2 . Because HCl and HF are highly reactive, surface-atmospheric buffering has been proposed to explain their abundance via gas-solid equilibria with mineral phases commonly found in alkaline basalts (which demonstrate mineralogy consistent with that inferred by surface XRF measurements), via net reaction such as (Fegley *et al.* 1997):



Similarly, mineral assemblages of oxides may buffer key atmospheric parameters such as the near-surface oxygen fugacity f_{O_2} (Fegley *et al.* 1997; Fegley 1997) and C-O-S equilibria, for which the f_{O_2} may regulate (for example) the near-surface $\text{H}_2\text{O}/\text{H}_2$, CO_2/CO , and SO_2/SO gas abundance ratios. Gas-phase equilibria in the lower atmosphere may in turn be used to indicate the relative stability of mineral phases at the surface (e.g., Zolotov 2018, 2019). Along with the near-surface near surface redox conditions and atmospheric abundances, surface mineralogy of Venus thus remains a key outstanding question for understanding chemical processes in the lower atmosphere.

4.2 Earth

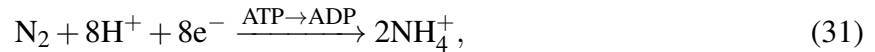
The determination of the Earth’s bulk atmospheric composition coincided with the chemical discovery of the molecular gases N_2 (1772), O_2 (1774), and CO_2 (1754) in the latter half of the 18th century and additional minor (e.g., Ar in 1894) and key trace species (e.g., O_3 in 1839) in the 19th and 20th centuries. The Earth’s atmosphere consists of 78% N_2 , 21% O_2 , and 0.934% Ar with a host of minor and trace species (see Table 3), including anthropogenic species. As noted by Lodders & Fegley (2011), the increasing number of detected atmospheric species in the terrestrial atmosphere throughout the 20th century can be attributed to advances in analytical techniques and also to the appearance of anthropogenic species (such as CFCs, HCCs, HCFCs, and HFCs) that were absent prior to the 20th century. The H_2O abundance is spatially and temporally variable (up to 4%) and Earth’s clouds are made of ice and/or liquid water. As an abundant and condensible species, the behavior of H_2O is of central importance for energy transfer, weather, and surface climate, and water vapour is the dominant greenhouse gas in the Earth’s atmosphere. Isotopic abundance comparisons between meteorites, comets, and the oceans and atmosphere suggest that the water inventory of the Earth may have been delivered primarily via volatile-rich planetesimals during its accretion, with a possible “late veneer” of comet-like material (e.g., see Dauphas *et al.* 2000; Morbidelli *et al.* 2000; Alexander *et al.* 2012; Marty 2012; Halliday 2013; O’Brien *et al.* 2018, and references therein).

Table 3: Composition of the Atmosphere of Earth

Gas	Abundance	Source	Sink
N ₂	78.08%	outgassing; bacterial denitrification	bacterial fixation; oxidation
O ₂	20.95%	photosynthesis	respiration and decay; oxidative weathering
H ₂ O	up to 4% (variable)	evaporation	condensation
³⁶ Ar	31 ppm	outgassing	none
⁴⁰ Ar	9303 ppm	⁴⁰ K decay; outgassing	none
CO ₂	410 ppm	outgassing, combustion	photosynthesis, oceans
CO	40 – 200 ppm (variable)	photochemistry, combustion	reaction with OH
CH ₄	1.8 ppm	biological, agricultural	reaction with OH
H ₂	0.5 ppm	H ₂ O photolysis	H atom escape
H ₂ O ₂	0.3 – 3	photochemistry	photochemistry
⁴ He	5 ppm	outgassing, radiogenic	escape
Ne	18.18 ppm	outgassing	none
Kr	1.14 ppm	outgassing	none
Xe	87 ppb	outgassing	none
N ₂ O	330 ppb	biology, agriculture, combustion	stratospheric photolysis
NO _x	30-300 ppt	combustion, biology	photolysis, photochemistry
NH ₃	0.1-3 ppb	biology	wet & dry deposition
HNO ₃	0.04-4 ppb	NO _x photochemistry	rainout
O ₃	10-100 ppb	photochemistry	photochemistry
HCl	1 ppb	derived from sea salt aerosols; volcanism	rainout
OCS	400-520 ppt (variable)	biology, volcanism, anthropogenic	photodissociation, biology
other S-gases ^a	≤ 260 ppt	biology, combustion, volcanism	photooxidation
HCCs ^b	700 ppt	anthropogenic	reactions with OH
CFCs ^c	818 ppt	anthropogenic	stratospheric photolysis
HCFCs ^d	309 ppt	anthropogenic	reactions with OH
HFCs ^e	218 ppt	anthropogenic	reactions with OH
other halocarbons ^f	≤ 200 ppt	anthropogenic	stratospheric photolysis

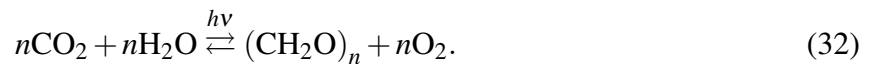
Table adapted after abundances and sources/sinks compiled in Lodders & Fegley (1998), with updates for anthropogenic greenhouse gas (CO₂, CH₄, N₂O) and halocarbon trace gas abundances from the NOAA ESRL Global Monitoring Laboratory (<https://www.esrl.noaa.gov/gmd/>). ^aSO₂, H₂S, CS₂, (CH₃)₂S. ^bCH₃Cl, CH₂Cl₂, CH₂ClCH₂Cl, CHCl₃, C₂H₅Cl, CHClCCl₂, CH₃CCl₃. ^cCCl₂F₂ (CFC-12), CCl₃F (CFC-11), C₂Cl₃F₃ (CFC-113), CClF₃ (CFC-13), C₂Cl₂F₄ (CFC-114), C₂ClF₅ (CFC-115). ^dCHClF₂ (HCFC-22), C₂H₃Cl₂F (HCFC-141b), C₂H₃ClF₂ (HCFC-142b), CHCl₂F (HCFC-21) ^eCH₂FCF₃ (HFC-134a), C₂HF₅ (HFC-125), CH₂F₂ (HFC-32), C₂H₃F₃ (HFC-143a), C₂H₄F₂ (HFC-152a), C₃HF₇ (HFC-227ea), C₄H₅F₅ (HFC-365ma), C₃H₂F₆ (HFC-236fa) ^fCF₄, CCl₄, CH₃Br, CH₃I, C₂F₂, C₂Cl₄, CBrClF₂ (halon-1211), CBrF₃ (halon-1301), C₂F₂Br₂ (halon-2402).

Both carbon and nitrogen show fast, biologically-mediated cycles tied to slower cycles operating over geological timescales (e.g., Johnson & Goldblatt 2015). The abundant molecular nitrogen in the Earth’s atmosphere – ultimately the product of geologically recent volcanic outgassing – is relatively inert due to the strength of the $\text{N}\equiv\text{N}$ bond (+940 kJ/mol). However, nitrogen fixation (i.e., the conversion into ammonia, nitrates, or nitrites) can occur during combustion of fossil fuels or vegetation, or by lightning strikes that produce NO_x species. Biological fixation plays an even larger role via the bacterial nitrogenase reaction:



and serves as the primary sink for molecular nitrogen in the terrestrial atmosphere. The ammonium ion is converted to nitrates by nitrifying bacteria; these nitrates are then assimilated into plants or converted back into N_2 by denitrifying bacteria, completing the cycle. Even without this recycling, the large reservoir of atmospheric nitrogen would make it stable over $\sim 10^7$ years; with recycling and outgassing sources (e.g., Sano *et al.* 2001) nitrogen is abundant in Earth’s atmosphere over geological timescales. A historical chronology of the development of our present-day understanding of the terrestrial nitrogen cycle can be found in the review of Galloway *et al.* (2013).

The abundances of O_2 and CO_2 in the Earth’s atmosphere are coupled. The ultimate source of molecular oxygen (O_2) in the Earth’s atmosphere is photosynthesis, represented by the net reaction:

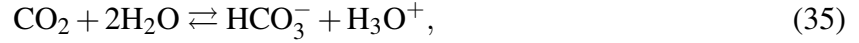
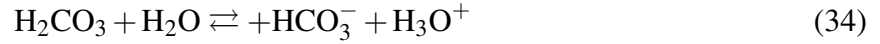


This reaction is reversible via respiration, so the accumulation of oxygen requires the burial and sequestration of organic carbon (e.g., Catling & Claire 2005; Duncan & Dasgupta 2017), a process that appears to have played a role in the gradual rise of atmospheric oxygen during the so-called Great Oxygenation Event near 2.3-2.4 Ga (e.g., see review in Lyons *et al.* 2014).

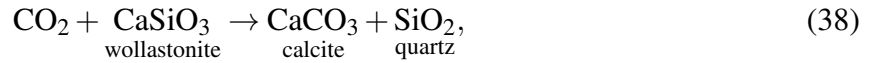
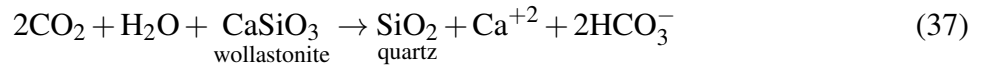
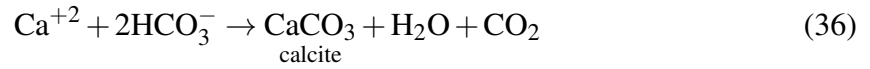
Photosynthesis also serves as a short-term sink for carbon dioxide. The CO_2 concentration shows an intra-annual variation of about 5 ppm per year corresponding to the seasonal uptake of CO_2 during northern hemisphere spring and summer (the growing season for most land vegetation on Earth), followed by the release of CO_2 back into the atmosphere during northern hemisphere fall and winter (see Figure 3). Volcanic emission of carbon dioxide is dwarfed by anthropogenic emissions (e.g., Burton *et al.* 2013), which are primarily responsible for the observed inter-annual increase of CO_2 from ~ 280 ppm in 1800 to ~ 410 ppm in 2020.

Other sinks for atmospheric CO_2 include the oceans, which represent a significantly larger reservoir (38,00 Gt) for carbon than the atmosphere (860 Gt; Friedlingstein *et al.* 2020). For example, rising atmospheric CO_2 concentrations from anthropogenic emission (Figure 3) drives

chemical equilibria such as (cf. Archer *et al.* 2009)



leading to increasing acidity (i.e., lower pH) in the Earth's oceans (e.g., Caldeira & Wickett 2003). Moreover, carbonates are precipitated by organisms to yield shell materials or produced by the chemical weathering of rocks via reactions such as



wherein they may be subducted and returned to the atmosphere as CO_2 via volcanic outgassing (e.g., Plank & Manning 2019). This carbonate-silicate cycle plays an important role in regulating the CO_2 abundance (and thus planetary temperature) over geological timescales. Moreover, sedimentary carbonates and kerogen together give a lithospheric carbon reservoir of $\sim 10^8$ Gt, vastly more than is present in the hydrosphere and atmosphere. The sequestration of carbon into lithospheric reservoirs represents a key difference from Venus, for which – lacking interaction with active hydrologic and biological cycles – the carbon inventory appears to reside in the atmosphere (see Figure 2).

The temperature increase of the Earth's stratosphere (15-50 km; see Figure 1) is due to the absorption of ultraviolet sunlight by ozone. The role of ozone as the absorber responsible for the UV cutoff in the solar spectrum was first proposed by Walter Noel Hartley in 1880, based upon comparison with experimental studies of O_3 (Hartley 1881). In their subsequent observations, Fowler & Strutt (1917) confirmed this result by identification of O_3 absorption bands in stellar and solar spectra, and suggested that the ozone was distributed in the upper atmosphere. The invention of the Dobson spectrometer (Dobson & Harrison 1926) provided a method for regular measurement of the atmospheric column density of O_3 . In 1930, Sydney Chapman proposed a

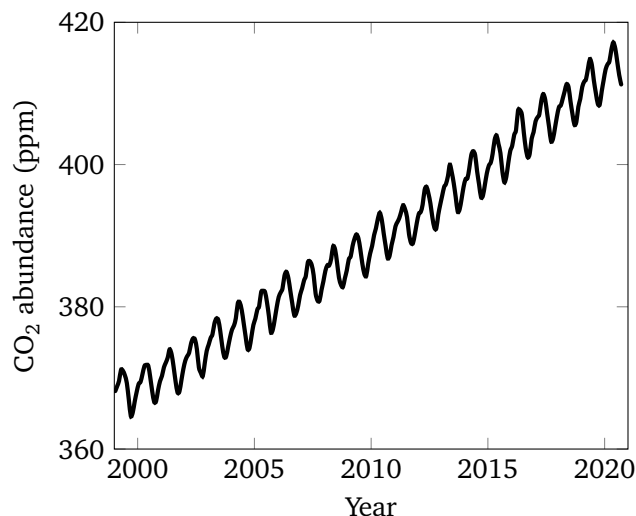


Figure 3: Abundance of CO₂ in the Earth's atmosphere from 2000-2020, showing seasonal variability and the anthropogenic inter-annual increase. Monthly data for the Mauna Loa observatory from the Scripps CO₂ Data Program (Keeling & Keeling 2017).

series of reactions to explain the behavior of ozone in the stratosphere (Chapman 1930):



The scheme shown here omits the slow Chapman reaction $\text{O} + \text{O} \xrightarrow{\text{M}} \text{O}_2$. Moreover, the O atom produced by ozone photolysis (reaction 41) may recombine with another O₂ molecule to produce O₃ (i.e., repeating reaction 40). In this case, as noted by Yung & DeMore (1999), there is no net change in O_x for the above sequence of reactions; stratospheric ozone is thus effective at blocking ultraviolet radiation and converting it into thermal energy.

By the mid-20th century, it was recognized that oxygen-only Chapman chemistry by itself predicted stratospheric ozone abundances greater than what was observed. The search for additional O₃ loss pathways led to the discovery of key catalytic processes in the stratosphere (Bates & Nicolet 1950; Norrish & Wayne 1965a,b). Ozone is readily destroyed by reactions with free radical species such as Cl·, Br·, and OH·, and HO_x, NO_x, ClO_x, and BrO_x catalytic cycles play an important role in the Earth's stratosphere.

The relative importance of a particular catalytic cycle varies with altitude and depends not only

upon reaction kinetics but also upon the number of times a cycle may repeat before the catalyst is lost to other processes (i.e., the *chain rate*; see Lary 1997). In general there are two basic net reaction schemes for ozone loss. In the middle stratosphere, the dominant type of scheme is



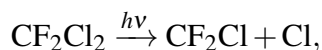
which can begin with either reaction and where $X = OH, Cl, Br,$ or NO . In the lower stratosphere (where the abundance of atomic O is relatively low and the abundance of O_3 is relatively high) the most effective catalytic cycle can be represented by the net reaction scheme



Additional reactions based upon this scheme can also play a role, including reactions among or between oxides (XO) such as $HO_2, ClO, BrO,$ and NO_2 (e.g., Lary 1997):



Enhanced catalytic destruction of ozone occurs in polar regions, where very low temperatures and the development of the polar vortex promote the formation of polar stratospheric clouds (PSCs). Surface reactions that occur on PSC particles produce Cl radicals than can readily react with ozone (e.g., via reactions 43 and 46). For similar reasons, anthropogenic emission of halocarbons has contributed to increased catalytic destruction of stratospheric ozone. These gases are destroyed by UV photolysis such as that for CFC-12:

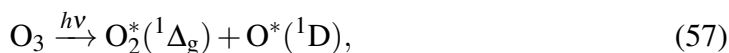


which produces Cl radicals in the stratosphere. Although a handful of halocarbon species (such as CH₃Cl) occur naturally, the abundances of CFCs, HCFCs, HFCs, and HCCs in Table 3 are almost entirely anthropogenically produced. CFCs are relatively inert and so survive into the stratosphere until they are destroyed by photolysis. As an alternative, many of the compounds proposed and developed to replace CFCs include hydrogen (HCFCs and HFCs). This gives them much shorter atmospheric residence times because they are subject to oxidation by OH in the troposphere (see below). In response to control measures such as the Montreal Protocols (signed in 1989), the atmospheric concentrations of the CFCs listed in Table 3 have decreased after 1995, whereas increased usage and emission has generally (aside from latitudinal and seasonal effects) increased the atmospheric concentrations of most HCFCs and HFCs.

As in the stratosphere, chemistry in the troposphere depends upon the abundances and reaction chemistry of key minor and trace species. Foremost among these is the reactive hydroxyl radical (OH), which effectively controls the atmospheric lifetimes of most minor or reactive species in the Earth's troposphere. Even though the concentration of OH is $\sim 10^6$ molecules cm⁻³ (Wayne 2000), it is the dominant oxidizing agent in the troposphere (for comparison, the number density of the Earth's atmosphere at sea level is $\sim 10^{19}$ molecules cm⁻³). For example, a dominant loss pathway for tropospheric CO and CH₄ (and higher hydrocarbons) is rapid reaction with OH, e.g.,



The primary formation pathway for hydroxyl is the the photolysis of O₃ followed by reaction of the excited oxygen atom with water:



Quenching of excited O may occur to produce a ground state atom of O, but free ground state oxygen atoms will produce ozone (via reaction 40), allowing for recycling. If present, NO₂ derived from natural (primarily lightning) or anthropogenic (primarily fossil fuel combustion) sources can also undergo photolysis via



to provide a free oxygen atom for the production of tropospheric ozone and the formation of photochemical smog. Major outstanding questions about terrestrial atmospheric composition consider the abundance trends and formation and loss pathways of key reactive species, greenhouse gases, pollution sources, and aerosols; how chemical and physical processes in the troposphere and stratosphere will both shape and respond to changes in climate and atmospheric composition; and

quantifying chemical transport and exchange between different planetary reservoirs, including the surface and interior.

4.3 Mars

Early estimates of Mars' atmospheric properties in the 18th and 19th centuries were provided by telescopic observations of shifting surface features, clouds, and atmospheric variability now attributed to dust storms. By the mid-20th century, ground-based spectroscopic observations had confirmed the existence of CO₂, and studies of Martian clouds and polar caps suggested ~millibar surface pressures (e.g., Hess 1948; Kuiper 1952; Grandjean & Goody 1955; Kaplan *et al.* 1964). Improved constraints on composition (including the first confirmation of solid CO₂) and atmospheric pressure were provided by the *Mariner* missions (1964-1971), followed by the first *in-situ* measurements of the atmosphere by the *Viking 1* and *Viking 2* landers (1976). Since then, numerous lander, rover, and orbiter missions alongside ongoing ground-based observations have provided information about the composition and climate of Martian atmosphere, including missions specifically equipped to explore the climate history of Mars, such as the *Curiosity* rover (2012), the *Phoenix* lander (2008) and orbiters including *Mars Reconnaissance Orbiter* (2006), *Mangalyaan* (2014), *MAVEN* (2014), and the *ExoMars Trace Gas Orbiter* (2016).

The composition of the Martian atmosphere is summarized in Table 4. The thin and cold atmosphere of Mars consists primarily of CO₂ (95.3%) with small amounts of N₂ (2.7%) and Ar (1.6%), and a number of minor species produced from photochemical reactions. With an average surface temperature near 214 K and surface pressures near 6-10 millibar, Mars surface conditions are below the triple point for both H₂O (273.16 K, 6.1 mbar) and CO₂ (216.6 K, 5.2 bar) so that liquid water and liquid carbon dioxide are both unstable, even at equatorial or summer daytime highs near 300 K. Both CO₂ and H₂O can produce frost on the Martian surface and commonly form thin clouds over a wide range of altitudes (Pollack *et al.* 1977; Pearl *et al.* 2001; Clancy *et al.* 2003; Montmessin *et al.* 2006; Whiteway *et al.* 2009; Määttänen & F. 2021). Water ice also forms clouds above the polar regions during local fall and winter (the “polar hood”), and around Mars' high shield volcanoes (e.g., Leovy *et al.* 1973; Pollack *et al.* 1977; Benson *et al.* 2011).

Table 4: Composition of the Atmosphere of Mars

Gas	Abundance	Source	Sink
CO ₂	95.32%	outgassing, sublimation	condensation
N ₂	2.7%	outgassing	atmospheric escape
Ar	1.6%	outgassing	none
O ₂	0.17% ^a	CO ₂ photolysis	photoreduction
CO	0.08%	CO ₂ photolysis	photooxidation
H ₂ O	0.03% (variable)	sublimation, desorption	condensation, adsorption
H ₂	15 ppm ^b	H ₂ O photolysis	atmospheric escape
NO	~100 ppm	photochemistry	photochemistry
Ne	2.5 ppm	outgassing	none
Kr	0.3 ppm	outgassing	none
Xe	0.08 ppm	outgassing	none
O ₃	0.02-0.2 ppm	photochemistry	photochemistry
H ₂ O ₂	23 ppb (variable) ^c	photochemistry	photodissociation
CH ₄	0-7 ppb	unknown	photochemistry, unknown

Table adapted after Lodders & Fegley (1998), with updates from the literature where indicated. ^aFranz *et al.* (2017) *Curiosity* SAM instrument suite; ^bKrasnopolsky & Feldman (2001); ^cusing mean column density from Encrenaz *et al.* (2004); ^dWebster *et al.* (2018) report a background level of 0.4 ppb based upon *Curiosity* Tunable Laser Spectroscopy measurements (see also Villanueva *et al.* 2013), whereas no CH₄ was detected by the ExoMars Trace Gas Orbiter (Korablev *et al.* 2019).

Despite the instability of liquid water at the surface of Mars today, starting with the apparent fluvial geomorphology revealed by *Mariner 9* (1971-1972), there is abundant geological and geochemical evidence that liquid water shaped Mars surface features in the distant past (e.g., Clifford 1993; Carr 1996; Bibring *et al.* 2006; Ehlmann *et al.* 2008, 2011). This has led to ongoing research exploring the conditions and mechanisms that could produce the observed surface features and mineralogy, and studies of the early climate history and evolution of the Martian atmosphere. These studies, along with observations of the upper atmosphere and exosphere, suggest extensive atmospheric loss that has transformed a warm and wet climate to the cold and dry planet we find today (Pollack *et al.* 1987; Jakosky & Phillips 2001; Jakosky *et al.* 2017, 2018). The water inventory on Mars is now mostly present as ice sequestered in the polar caps and the subsurface, and hydrated mineral deposits in the crust (e.g., Scheller *et al.* 2021; Wernicke & Jakosky 2021).

In the present-day atmosphere of Mars, large surface pressure variations are caused by the 25° tilt of Mars' axis which yields large temperature variations and the corresponding seasonal deposition and sublimation of significant amounts of CO₂ ice (and to a lesser extent H₂O ice) in

the polar regions, summarized by the net reaction



for which the equilibrium vapour pressure of CO_2 is ~ 1 mbar at 140 K. Because CO_2 is the primary component of the atmosphere, this seasonal cycle provides significant interannual variability: surface pressures drop as more CO_2 is deposited into polar ice. For example, the *Viking* landers and *Curiosity* rover measured surface pressures ranging from 7 mbar to 10 mbar corresponding to seasonal behavior of the polar caps (Hess *et al.* 1977, 1980; Kelly *et al.* 2006; Trainer *et al.* 2019).

As on Venus, atmospheric CO_2 on Mars is also subject to loss via photolysis:

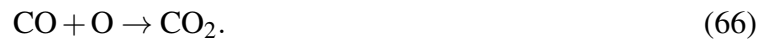


A key difference is that this photolysis can occur throughout the entire Martian atmospheric column down to the surface. Thus, Mars has the same stability problem as Venus, and CO_2 would be gradually removed from the atmosphere unless there is an efficient method for recycling production. Moreover, observations of CO (Kaplan *et al.* 1964) and O_2 (Barker 1972) show abundances lower than expected, suggesting a conversion mechanism back into CO_2 (e.g., see Nair *et al.* 1994).

The presence of atmospheric H_2O ($\sim 0.03\%$) allows for HO_x catalytic cycles that recycle CO_2 . For example, McElroy & Donahue (1972) showed that CO_2 recombination can be catalyzed by OH radicals, which may be produced by the photolysis of H_2O via



which can initiate a series of reactions:



The H atom produced by H_2O photolysis can also react with HO_2 to produce H_2 and O_2 :



The hydrogen produced in this way diffuses from the lower atmosphere to the upper atmosphere, where ionospheric reactions produce H atoms that are subject to thermal escape. This is supported by spectroscopic observations of H atoms in Mars' exosphere, and consistent with the escape of

449 H₂O in stoichiometric proportions (due to self-regulating photochemical processes; see Yung &
450 DeMore 1999) over long periods of Martian history (Jakosky *et al.* 2015; Chaffin *et al.* 2017).

HO_x chemistry also plays a role in regulating the abundances of other key species such as ozone (O₃) and hydrogen peroxide (H₂O₂) in the Martian atmosphere (e.g., Nair *et al.* 1994; Lefèvre *et al.* 2008). As on Earth, ozone is produced by the sequence of reactions,



451 and is readily destroyed by H (a product of H₂O photolysis):



452 This relationship yields an inverse correlation between the O₃ abundance and that of HO_x-producing
453 water vapor, consistent with model-data comparisons and *Mars Express* observations of seasonal
454 variations that show relatively high O₃ abundances during Mars' northern winter (Lefèvre *et al.*
455 2008). Hydrogen peroxide (H₂O₂), proposed as an oxidizing agent of the Martian regolith (Oyama
456 & Berdahl 1977) and detected by microwave spectroscopy (Clancy *et al.* 2004; Encrenaz *et al.*
457 2004), is produced from HO_x via the reaction



458 The photolysis of H₂O₂ produces hydroxyl radicals



459 The reactions above are expected to yield a positive correlation between the H₂O₂ abundance and
460 that of water vapor. At high H₂O abundances, H₂O₂ photolysis is an important source of OH
461 radicals in HO_x catalytic cycles beginning with reaction (63) that recycle CO and O back to CO₂.

462 The reported detections of trace and variable amounts of CH₄ by ground-based and *Mars Ex-*
463 *press* infrared spectroscopy and the *Curiosity* rover and the non-detection reported by the ExoMars
464 Trace Gas Orbiter have been a subject of particular interest and debate (e.g., see Formisano *et al.*
465 2004; Mumma *et al.* 2009; Zahnle *et al.* 2011; Krasnopolsky 2012; Webster *et al.* 2013, 2015,
466 2018; Korablev *et al.* 2019). In the upper atmosphere (> 70 km) CH₄ is readily destroyed by UV
467 photolysis. In the lower atmosphere, CH₄ photolysis is shielded by UV absorption from CO₂, but
468 is subject to oxidation (as on Earth) by OH radicals:



Taken together, these processes yield an CH_4 atmospheric lifetime of ~ 300 years (e.g., Villanueva *et al.* 2013). Shorter period spatial and/or seasonal variations in the CH_4 abundance in Mars' atmosphere would thus rely upon atmospheric production and loss processes that remain poorly understood. A number of different methane sources have been proposed, including volcanism, microbial activity, or chemical reactions associated with metamorphism. This methane is plausibly destroyed by some yet-unidentified oxidizing agent such as H_2O_2 . More generally, surface-atmosphere interactions and heterogeneous chemistry on ice or dust grains may play an important role in the oxidation of the Martian regolith and atmosphere. For example, model-data comparisons of Martian photochemistry suggest that heterogeneous chemistry is needed explain the relationship between observed gas abundances and photochemical model predictions (Anbar *et al.* 1993; Krasnopolsky 1993; Atreya & Gu 1994; Krasnopolsky 2006; Lefèvre *et al.* 2008). The results of the *Viking* lander biological experiments are also consistent with the presence of a strong oxidizing agent (Oyama & Berdahl 1977; Navarro-González *et al.* 2010; Encrenaz *et al.* 2012). The behavior of perchlorate (ClO_4^-) compounds, first detected at the *Phoenix* lander site (Hecht *et al.* 2009), may provide further clues. The redox chemistry of the Martian regolith and near-surface atmosphere (e.g., Spiga 2019) – and its relationship to the climate history of Mars – remains an subject of active observational, experimental, and theoretical investigation.

5 Giant planet atmospheres

The atmospheres of the gas giant planets exist as massive molecular envelopes consisting mostly of molecular hydrogen (H_2) and helium (He) captured as primary atmospheres from the solar nebula during planetary formation. In contrast to the terrestrial planets, the gas giants have no solid planetary surface. For this reason, their radii are defined adopting an atmospheric reference pressure of 1 bar (see Table 1), with pressures and temperatures increasing with depth into the troposphere. The atmospheric profiles for the gas giant planets down to the ~ 20 bar level are shown in Figure 4.

The observed chemical abundances in the atmospheres of the giant planets are summarized in Table 5. To a rough first approximation, the giant planet atmospheres are protosolar in composition, with varying enhancements in heavy elements (i.e., elements heavier than He) such as carbon, nitrogen, and oxygen, present as hydrides. The low observed abundances of NH_3 , H_2O , and H_2S on Saturn, Uranus, and Neptune are attributed to their sequestration into cloud layers a deeper atmospheric levels. In all four giant planets, the observed atmospheric chemistry is shaped by various chemical and physical processes including thermochemical equilibrium, reaction kinetics and atmospheric mixing, cloud formation, and photochemistry.

Table 5: Composition of Giant Planet Atmospheres

Gas	Protosolar ^a	Jupiter	Saturn	Uranus	Neptune
<i>Major species</i>					
H ₂	83.2%	86.4%	88%	~82.5%	~80%
He	16.6%	13.6%	11.9% ^d	15.2%	19.0%
<i>Condensible Species</i>					
CH ₄	602 ppm	2050 ppm ^b	4500 ppm	2.3%	2-4% ^e
NH ₃	145 ppm	351 ppm ^c	159 ppm	< 100 ppb	< 600 ppb
H ₂ O	882 ppm	2500 ppm ^c	2-200 ppb	-	-
H ₂ S	29 ppm	77 ppm ^b	< 0.4 ppm	< 0.8 ppm	< 3 ppm
<i>Deuterated Species</i>					
HD		45 ppm	110 ppm	148 ppm	192 ppm
CH ₃ D		0.20 ppm	0.39 ppm	8.3 ppm	12 ppm
<i>Noble Gases</i>					
Ne	289 ppm	21 ppm	-	-	-
Ar	6.5 ppm	16 ppm	-	-	-
Kr	3.4 ppb	8 ppb	-	-	-
Xe	0.4 ppb	0.8 ppb	-	-	-
<i>Disequilibrium and Photochemical Species</i>					
PH ₃	0.5 ppm	0.7 ppm	4.5 ppm	< 1.1 ppb ^f	-
GeH ₄	7.9 ppb	0.7 ppb	0.4 ppb	-	-
AsH ₃	0.4 ppb	0.22 ppb	2.1 ppb	-	-
CO		1 ppb	1.4 ppb	< 40 ppb	0.65 ppm
CO ₂		5-35 ppb	0.3 ppb	< 0.3 ppb	< 0.5 ppb
HCN		60 ppb	< 4 ppb	< 15 ppb	0.3 ppb
C ₂ H ₂		0.11 ppm	0.30 ppm	10 ppb	60 ppb
C ₂ H ₄		7 ppb	0.2 ppb	-	-
C ₂ H ₆		5.8 ppm	7.0 ppm	10 ppb ^g	1.5 ppm
C ₄ H ₂		0.3 ppm	0.09 ppb	0.16 ppb ^g	detected
CH ₃ C ₂ H		2.5 ppb	0.6 ppb	0.25 ppb ^g	0.12 ppb

Abundances given as volume mixing ratios following the compilations of Lodders & Fegley (1998); Lodders & Fegley (2011) and de Pater & Lissauer (2015), with updates from the literature where indicated. ^aEstimated abundances in a protosolar-composition gas based upon the protosolar elemental abundances in Lodders (2020). The protosolar H₂O abundance is calculated assuming the prior removal of ~20% of the oxygen inventory into rock-forming oxides. ^bWong *et al.* (2004); ^cLi *et al.* (2020); ^dConrath & Gautier (2000); ^eIrwin *et al.* (2019); ^fTeanby *et al.* (2019); ^gBurgdorf *et al.* (2006).

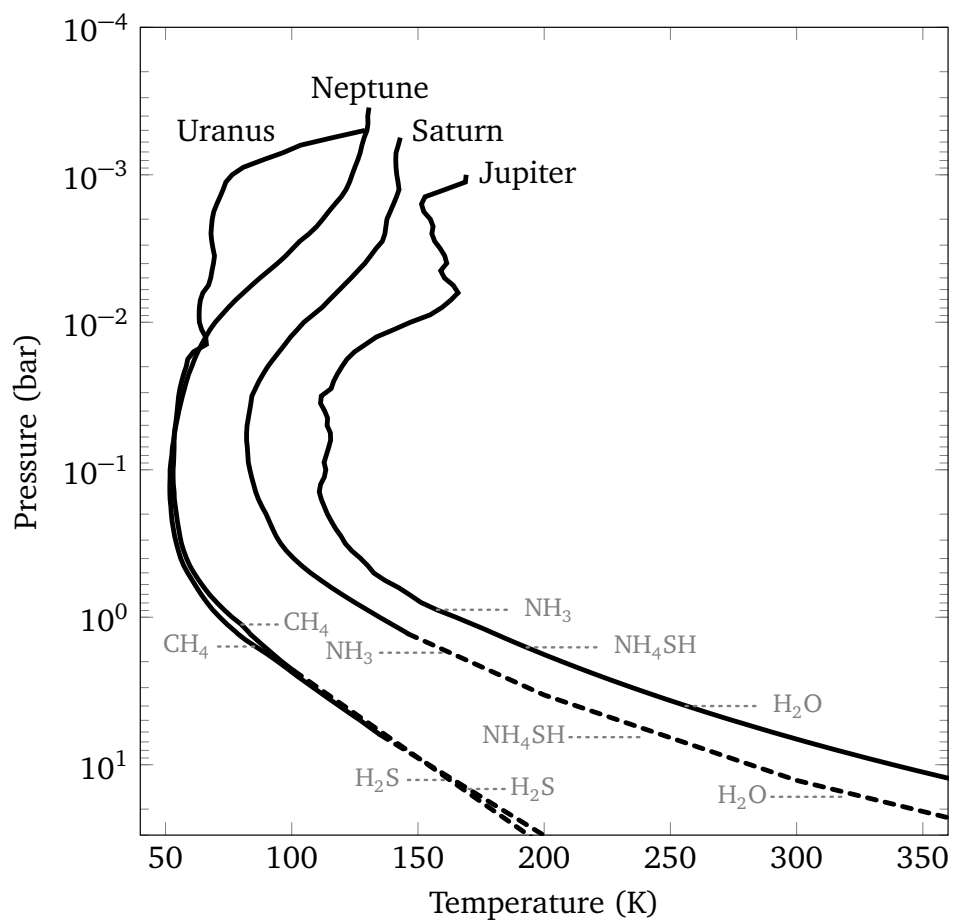


Figure 4: Atmospheric profiles for Jupiter, Saturn, Uranus, and Neptune, derived from *Voyager* radio occultation data (Lindal *et al.* 1985; Lindal 1992) and *in situ* observations of Jupiter's atmosphere by the *Galileo* entry probe (Seiff *et al.* 1998). The dashed lines are extensions of adiabatic profiles into the deep troposphere. The horizontal dotted lines denote the pressure and temperature of the cloud base (i.e., the greatest depth at which equilibrium condensation occurs) for different condensates (labeled) along each profile. For Uranus and Neptune, the NH_3 , NH_4SH , and H_2O cloud layers are expected to condense at higher pressures and temperatures than shown here.

It is convenient to further divide the giant planets into two categories: the larger *gas giants* Jupiter and Saturn and the smaller *ice giants* Uranus and Neptune. The differences are most readily distinguished by a comparison of the inferred interior structures of the giant planets, as illustrated in Figure 5. Gas-rich Jupiter and Saturn are more massive ($318 M_E$ and $95 M_E$, respectively), larger ($11.2 R_E$ and $9.5 R_E$), and consist mostly of hydrogen and helium, with relatively small cores of rock and ice. Although Uranus ($14.5 M_E$, $4.0 R_E$) and Neptune ($17.1 M_E$, $3.9 R_E$) likewise possess hydrogen-rich molecular envelopes, these planets are significantly smaller and appear to contain a much greater proportion of “ice-forming” (e.g., C, N, O) and rocky (e.g., Mg, Si, Fe) elements. Here we will discuss the atmospheric chemistry of each of these sub-categories in turn, with a focus on tropospheric abundances and the processes shaping the observed compositions of giant planet atmospheres.

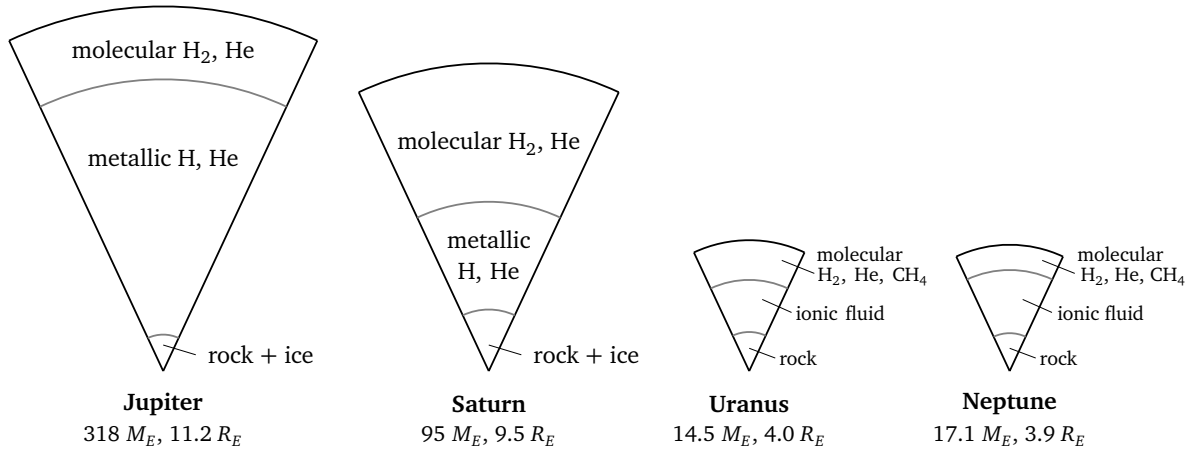


Figure 5: Simplified schematic cross-sections (drawn to scale) of the interior structures of Jupiter, Saturn, Uranus, and Neptune. See Stevenson (1982); Hubbard *et al.* (1995); Guillot (1999); Guillot *et al.* (2004); Marley & Fortney (2007) for details.

5.1 Jupiter and Saturn

The low densities of Jupiter (1.3 g cm^{-3}) and Saturn (0.7 g cm^{-3}), along with the presence of hydrides (e.g., CH_4 , NH_3), led early observers and theorists to conclude that these giant planets consist mostly of hydrogen and have bulk compositions roughly similar to that of the Sun (e.g., Jeffreys 1924; Wildt 1932). Moreover, advances in our understanding of high-pressure materials, including the prediction of metallic hydrogen (Wigner & Huntington 1935) yielded early models of Jupiter and Saturn that consisted of H and He and included a metallic hydrogen layer (e.g., Brown 1950; Ramsey 1951; Demarcus 1958; Peebles 1964). High-pressure experiments and models, along with spacecraft measurements of the gravitational field have provided additional constraints for models of interior structure and composition. Jupiter and Saturn both appear to possess dense core of rock and possibly ice, an overlying mantle of fluid metallic hydrogen (stable

at pressures above ~ 2 Mbar), and an outer molecular H_2 -He envelope (see Figure 5) of which only the uppermost portions are directly observable by remote-sensing or *in-situ* methods.

Far-infrared measurements show that both Jupiter and Saturn emit nearly twice as much energy than they receive from the Sun (Low 1966) suggestive of convecting interiors (Peebles 1964; Hubbard 1968, 1969). The composition of their visible atmospheres is thus expected to be generally representative of bulk atmospheric composition. For example, the tropospheric abundances of CH_4 , NH_3 , H_2S , and H_2O are generally assumed to represent the elemental abundances of the C, N, S, and the majority of planetary O (e.g., see Figure 6). However, recent *Juno* measurements of Jupiter’s gravity field suggest the possibility of a diluted core and non-uniform heavy element mixing throughout the planet as a whole (e.g., Debras & Chabrier 2019; Wahl *et al.* 2017). The global distribution of heavy elements – and the extent to which tropospheric abundances are representative of a bulk planetary inventory – thus remain outstanding questions for observational and theoretical study.

Atmospheric abundances for Jupiter and Saturn are given in Table 5, derived mostly from ground- and spacecraft-based infrared observations (in particular, *Voyager 1-2*, *Galileo*, and *Juno* to Jupiter; *Voyager 1-2* and *Cassini* to Saturn). The *Galileo* entry probe also provided *in situ* mass spectrometer measurements of Jupiter’s atmosphere down to 22-bar level, showing element-to- H_2 enrichments of $\sim 2 - 4\times$ relative to a protosolar composition for C, N, S, Ar, Kr, and Xe (Mahaffy *et al.* 2000; Wong *et al.* 2004) and depletions in others (Ne, He, and O; see Figure 6). However, the entry probe entered Jupiter’s atmosphere in a “hot-spot” region characterized by low cloud opacity, low abundances of cloud-forming species, high thermal ($5\ \mu\text{m}$) emission, and a water abundance that was still increasing with depth when the probe signal was lost. More recently, microwave observations (which probe as deep as ~ 100 bar) by the *Juno* spacecraft suggest a deep H_2O abundance of 2500 ppm, corresponding to an oxygen enrichment roughly similar to that for other heavy elements (e.g., see Figure 6; Li *et al.* 2017; Li *et al.* 2020). On both planets, the depletion in He relative to a protosolar composition is attributed to the removal of He from the molecular envelope into the metallic H-He layer. A similar effect is observed for Ne on Jupiter, plausibly due to the incorporation of Ne into He droplets separating out of H-He metal (Roulston & Stevenson 1995; Fortney & Hubbard 2003).

A number of species condense in the upper tropospheres of both planets, producing (from the bottom up) an H_2O cloud consisting of aqueous solution and/or water ice, ammonium hydrosulfide (NH_4SH), and NH_3 ice (see Figure 4). Each cloud layer removes condensable species from the atmosphere and introduces cloud particles that contribute to opacity. For example, the bright zones of Jupiter’s banded structure appear to be caused by icy NH_3 clouds. Removal by cloud formation also explains the low observed abundances of NH_3 , H_2O , and H_2S in the stratosphere and upper troposphere Saturn, at altitudes above the condensation levels for each of these species. Abundance estimates from microwave observations predict higher abundances of NH_3 , H_2O , and

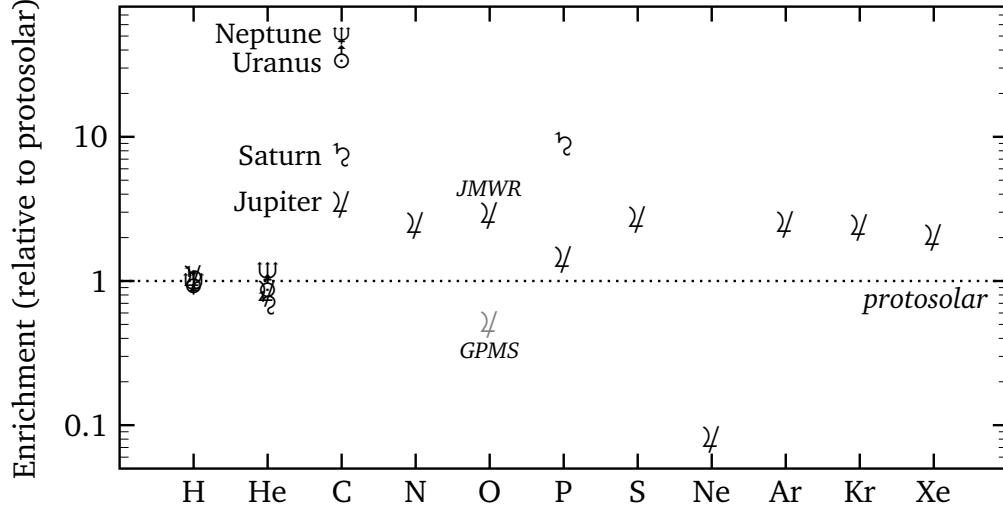


Figure 6: Observed element abundance inventories in the giant planets relative to a protosolar-composition gas (dotted line). Protosolar abundances are derived from Lodders (2020) assuming H as H_2 , C as CH_4 , N as NH_3 , O as H_2O , P as PH_3 , and S as H_2S . A limited number of elements are shown for Saturn (H, He, C, P), Uranus (H, He, C), and Neptune (H, He, C), as other species remain undetected or have been removed by condensation in the upper troposphere. For Jupiter, the H_2O abundance measured by the *Galileo* Probe Mass Spectrometer (GPMS) (Wong *et al.* 2004) and the *Juno* Microwave Radiometer (JMWR) (Li *et al.* 2017; Li *et al.* 2020) are shown for comparison.

H_2S at pressures between 5-10 bar, below their respective cloud layers (de Pater & Mitchell 1993). Heavy element abundances in Saturn’s deep atmosphere are thus estimated from measurements of CH_4 and PH_3 (e.g., Visscher & Fegley 2005), which show element-to- H_2 enhancements of $\sim 7\text{-}9\times$ relative to a protosolar composition.

The equilibrium condensate model was first developed to explain and identify tropospheric cloud formation of H_2O , NH_4SH , and NH_3 cloud layers on Jupiter and Saturn (Lewis 1969; Lewis & Prinn 1970; Weidenschilling & Lewis 1973; Atreya *et al.* 1996; Gierasch *et al.* 2000; Ingersoll *et al.* 2000). Additional cloud condensates (including, for example, Fe metal and Mg-silicates) are expected to form at higher pressures and temperatures in the deep atmospheres of both planets. This scenario is supported by several lines of evidence (e.g., see Lodders & Fegley 1994, 2006; Visscher *et al.* 2010a), including the detection of GeH_4 and absence of SiH_4 on Jupiter and Saturn (although $A_{\text{Si}} > A_{\text{Ge}}$), presumably due to the removal of Si into silicate clouds deeper in the atmosphere, and by the detection of H_2S in Jupiter’s atmosphere by the *Galileo* entry probe, which suggests removal of Fe into a deep cloud layer, as FeS formation would otherwise remove S from the gas phase above the ~ 700 K level (because $A_{\text{Fe}} > A_{\text{S}}$; Fegley & Lodders 1994; Lodders & Fegley 2002; Visscher *et al.* 2006). Assuming uniform protosolar elemental abundance ratios (e.g., Si/O), the condensation of rock-forming elements in the deep atmosphere sequesters $\sim 20\%$ of the total oxygen inventory in a protosolar-composition gas (Lodders 2004; Visscher & Fegley 2005; Visscher *et al.* 2010b; Lodders 2020), with the remainder mostly present as water vapour until H_2O

itself condenses in the upper troposphere.

A number of tropospheric species are present in abundances much greater than predicted by thermodynamic equilibrium. The two main disequilibrium processes in giant planet atmospheres are

- transport-induced quenching, which occurs when atmospheric mixing occurs faster than chemical reactions can act to maintain equilibrium, and
- photochemistry, which occurs when molecules are broken apart by stellar UV radiation that triggers subsequent chemical reactions.

The role of quench chemistry was first demonstrated for CO on Jupiter (Prinn & Barshay 1977). For species such as CO, PH₃, GeH₄, and AsH₃, observed abundances far in excess of thermodynamic predictions suggest rapid vertical mixing from warmer, deeper levels where each species has a greater abundance at an equilibrium maintained by fast reaction kinetics. However, departures from equilibrium occur at higher, cooler altitudes when vertical mixing occurs faster than chemical reactions can maintain equilibrium, effectively “quenching” the abundance of a molecular species at a fixed value throughout the upper troposphere (e.g., see Prinn & Barshay 1977; Fegley & Prinn 1985; Fegley & Lodders 1994; Visscher & Moses 2011; Wang *et al.* 2016; Visscher 2020). The behavior of these quenched species thus provides clues about the chemical composition down to \sim kilobar levels in giant planet atmospheres (Giles *et al.* 2017a; Grassi *et al.* 2020; Visscher 2020).

Photochemistry also plays an important role in the stratosphere and upper troposphere of the gas giant planets. For example, short wavelength ultraviolet photons ($\lesssim 100$ nm) are absorbed by H₂ photolysis in the upper stratosphere:



Methane is photolyzed (at $\sim 100 - 200$ nm) in the lower stratosphere via reactions such as



The products of these photolysis reactions can then combine in various ways to produce heavier hydrocarbons including C₂H₂, C₂H₄, C₂H₆, C₄H₂, and CH₃C₂H, many of which have been observed in the upper atmospheres of the giant planets (e.g., see Gladstone *et al.* 1996; Moses *et al.*

2000, 2005). For example, key reactions for the production of C₂ species include



which can undergo additional photolysis and recombination reactions to produce higher hydrocarbons. The products of hydrocarbon photochemistry diffuse downward and are eventually recycled back into CH₄ at deeper, warmer levels in the atmosphere, so that there is no net loss of methane with time.

Most UV photons are absorbed by H₂ photolysis in the upper stratosphere and CH₄ photolysis in the lower stratosphere via the reactions above. However, longer wavelength UV photons (> 150 nm) may penetrate into the upper troposphere to drive additional photochemical reactions involving NH₃, PH₃, and (to a lesser extent) H₂S:



Each of these reactions produces H atoms and a reactive radical that leads to the formation of additional N, P, and S species, respectively, eventually producing condensates such as hydrazine (N₂H₄), red phosphorus (P₄; identified as a chromophore candidate for the Great Red Spot; Prinn & Lewis 1975), and elemental sulfur (S₈; a yellow chromophore candidate). Moreover, coupled NH₃-PH₃ photochemistry (and to a lesser extent CH₃-NH₃ chemistry that may produce the observed HCN) occurs because these gases absorb UV photons at similar atmospheric levels. Tropospheric photochemistry is thus a potential source of aerosols and chromophores in the upper atmospheres of Jupiter and Saturn (e.g., Atreya *et al.* 1977; Kaye & Strobel 1983, 1984; Edgington *et al.* 1998, 1999; West *et al.* 2007; Visscher *et al.* 2009), although the specific composition of chromospheric compound(s) remains unresolved.

5.2 Uranus and Neptune

Uranus (discovered in 1781 by Sir William Herschel) and Neptune (discovered in 1846 by Johann Galle, based upon the predictions of Urbain LeVerrier) are the only major planets in our Solar System not known from antiquity. Compared to Jupiter and Saturn (and lacking the extent of gravitational compression found on Jupiter), the relatively higher densities of Uranus (1.33 g cm⁻³) and Neptune (1.64 g cm⁻³) suggest a bulk composition with a greater proportion of heavy elements

relative to H and He. Although CH₄ and molecular H₂ and a number of other planetary properties had been detected in both planets from ground-based observations in the early and mid-20th century (e.g., see Adel & Slipher 1934; Kuiper 1952; Herzberg 1952; Trafton 1981; Bergstrahl 1984), our understanding of the atmospheric chemistry of Uranus and Neptune was greatly advanced by the *Voyager 2* flybys of Uranus in 1986 and of Neptune in 1989 (e.g., for reviews see Fegley *et al.* 1991; Gautier *et al.* 1995; Moses *et al.* 2020).

The observed atmospheric abundances for Uranus and Neptune are given in Table 5. Notably, radio occultation and infrared spectroscopic measurements by *Voyager 2* indicate He/H ratios on both planets that are roughly similar to the protosolar value (Conrath *et al.* 1987, 1991). This is higher than observed on Jupiter and Saturn, because Uranus and Neptune lack any H-He metallic layer (their interior pressures are too low) that could give rise to He differentiation. Instead, interior models of Uranus and Neptune generally include a core of rocky material, an overlying ionic/fluid mantle with abundant ice-forming elements (C, N, O), and an outer molecular H₂-He-CH₄ envelope (e.g., see Figure 5 and Stevenson 1982).

Large enrichments in heavy elements are likewise demonstrated by the high measured CH₄ abundance on each planet, which is 50-100× the CH₄/H₂ abundance ratio in a protosolar composition gas. The preferential absorption of red light by methane is responsible for the characteristic blue color of each planet. The atmospheres of Uranus and Neptune are also cold enough to yield CH₄ (and possibly H₂S) cloud formation in the upper troposphere, consistent with ground-based and *Voyager 2* observations of aerosols and hazes in atmospheres that are otherwise relatively clear over a large range of observable altitudes (e.g., Smith *et al.* 1989; Stone & Miner 1989; West *et al.* 1991; Baines *et al.* 1995). Enhancements for other heavy elements (N as NH₃, O as H₂O, etc) are anticipated but not observed, plausibly due to their removal into clouds and/or sequestration into an ionic fluid layer deeper in the atmosphere.

As for Jupiter and Saturn, stratospheric CH₄ photochemistry on Uranus and Neptune produces a number of hydrocarbon products including CH₃, C₂H₂, C₂H₄, C₂H₆, C₄H₂, and CH₃C₂H, several of which have been observed on both planets (e.g., see Table 5 and review in Moses *et al.* 2020). These products are also susceptible to ultraviolet photolysis and condensation, contributing to haze formation in the lower stratosphere (e.g., Romani & Atreya 1988; Summers & Strobel 1989; Moses *et al.* 1992, 1995). In the troposphere, longer-wavelength ultraviolet radiation is expected to efficiently photolyze PH₃ and may lead to the production of P₂H₄ (Teanby *et al.* 2019). However, coupled C-N or P-N is not expected to play a significant role given the low upper-tropospheric abundance of NH₃.

Uranus displays a number of unique properties that are relevant for its atmospheric chemistry, including an obliquity of 97.9° between its rotation axis and orbital plane. Despite large variations in insolation over the course of a Uranian year, seasonal effects on hydrocarbon photochemistry are minimized due to poor mixing and long chemical lifetimes in the stratosphere (Moses *et al.*

2018). The internal heat flux from Uranus is also either very weak or nonexistent compared to the other giant planets, with a ratio of thermal radiation to absorbed solar energy of 1.06 ± 0.08 (Pearl *et al.* 1990). This heat source is plausibly explained by radiogenic heating from a $\sim 5M_E$ rocky core of chondritic composition (Pearl *et al.* 1990; Podolak *et al.* 1991).

For comparison, Neptune emits $2.6 \times$ more radiation than it receives from the Sun (2.61 ± 0.28 ; Conrath *et al.* 1991), which may drive more efficient tropospheric mixing than on Uranus. This behavior is consistent with differences the observed CO abundance on each planet: an upper limit of < 40 ppb on Uranus but as high as ~ 1 ppm on Neptune. Although the detection of CO in the stratosphere suggests an external source of CO, tropospheric CO has generally been attributed to an internal source. As demonstrated by Lodders & Fegley (1994) the observed disequilibrium abundance of CO may thus provides estimates of the oxygen abundance (as H_2O) in the deep atmosphere, via the net thermochemical reaction



For a given CH_4 abundance, the quenched abundance of CO mixed into the upper troposphere depends CH_4 -CO reaction kinetics, the rate of vertical mixing, and the deep H_2O abundance: more H_2O yields more CO. Following the conceptual approach of Prinn & Barshay (1977), chemical timescale and kinetics and transport modeling approaches yield constraints on the deep oxygen inventory of $250\text{--}650 \times$ protosolar on Neptune and an upper limit of $< 45\text{--}260 \times$ protosolar on Uranus (e.g., Fegley & Prinn 1985, 1986; Lodders & Fegley 1994; Cavalié *et al.* 2017; Moses *et al.* 2020). Similar transport-induced quenching could also yield disequilibrium abundances of other carbon- and nitrogen-bearing species such as CO_2 , N_2 , and HCN (detected at 0.3 ppb on Neptune) in the upper atmospheres of both planets, which would provide better constraints on atmospheric mixing processes. Improved estimates of the CO tropospheric abundance on Uranus would allow for improved constraints on the deep water abundance and differences between the deep compositions of Uranus and Neptune, which – along with interior structures – remain poorly known. In general, the element abundance inventories of the giant planets appear to show increasing heavy element enrichment and increasing O/C abundance ratios moving outward in the solar system, suggestive of significant H_2O and heavy element enrichments on Uranus and Neptune. Such abundance trends thus may serve as a key constraint for models describing the formation and evolution of such “ice giant” planets both inside and outside our solar system.

For further reading

- Chamberlain, J. W. & Hunten, D. M., 1989. *Theory of Planetary Atmospheres: An Introduction to Their Physics and Chemistry*. Vol. 36 in International Geophysics Series. Academic Press.
- Yung, Y. L. & DeMore, W. B., 1999. *Photochemistry of Planetary Atmospheres*. New York: Oxford University Press
- Wayne, R., 2000. *Chemistry of Atmospheres: An Introduction to the Chemistry of the Atmospheres of Earth, the Planets, and Their Satellites*. Oxford University Press
- Lewis, J. 2004. *Physics and Chemistry of the Solar System, 2nd ed.* Vol. 87, International Geophysics Series. Academic Press.
- Lodders, K. & Fegley, B., Jr. 2011. *Chemistry of the Solar System*. Cambridge: Royal Society of Chemistry

References

- Adams, W. S. and Dunham, J., T., 1932. Absorption Bands in the Infra-Red Spectrum of Venus. *Publications of the Astronomical Society of the Pacific*, 44, 243–245
- Adel, A. and Slipher, V. M., 1934. Concerning the Carbon Dioxide Content of the Atmosphere of the Planet Venus. *Physical Review*, 46, 240–240
- Alexander, C. M. O., Bowden, R., Fogel, M. L., Howard, K. T., Herd, C. D. K. and Nittler, L. R., 2012. The Provenances of Asteroids, and Their Contributions to the Volatile Inventories of the Terrestrial Planets. *Science*, 337, 721
- Allen, D. A. and Crawford, J. W., 1984. Cloud structure on the dark side of Venus. *Nature*, 307, 222–224
- Anbar, A. D., Leu, M. T., Nair, H. A. and Yung, Y. L., 1993. Adsorption of HO_x on aerosol surfaces: Implications for the atmosphere of Mars. *Journal of Geophysical Research*, 98, 10933–10940
- Archer, D., Eby, M., Brovkin, V., Ridgwell, A., Cao, L., Mikolajewicz, U., Caldeira, K., Matsumoto, K., Munhoven, G., Montenegro, A. and Tokos, K., 2009. Atmospheric Lifetime of Fossil Fuel Carbon Dioxide. *Annual Review of Earth and Planetary Sciences*, 37, 117–134
- Arney, G., Meadows, V., Crisp, D., Schmidt, S. J., Bailey, J. and Robinson, T., 2014. Spatially resolved measurements of H₂O, HCl, CO, OCS, SO₂, cloud opacity, and acid concentration in the Venus near-infrared spectral windows. *Journal of Geophysical Research (Planets)*, 119, 1860–1891
- Atreya, S., Owen, T. and Wong, M., 1996. Condensible volatiles, clouds, and implications for meteorology in the Galileo probe entry region: Jupiter is not dry! *Bulletin of the American Astronomical Society*, 28, 1133
- Atreya, S. K., Donahue, T. M. and Kuhn, W. R., 1977. The distribution of ammonia and its photochemical products on Jupiter. *Icarus*, 31, 348–355
- Atreya, S. K. and Gu, Z. G., 1994. Stability of the Martian atmosphere: Is heterogeneous catalysis essential? *Journal of Geophysical Research*, 99, 13133–13146
- Atreya, S. K., Pollack, J. B. and Matthews, M. S., 1989. *Origin and Evolution of Planetary and Satellite Atmospheres*. University of Arizona Press, Tucson
- Avice, G. and Marty, B., 2020. Perspectives on Atmospheric Evolution from Noble Gas and Nitrogen Isotopes on Earth, Mars & Venus. *Space Science Reviews*, 216, 36. 2003. 11431
- Baines, K. H., Hammel, H. B., Rages, K. A., Romani, P. N. and Samuelson, R. E., 1995. *Clouds and hazes in the atmosphere of Neptune*. 489–546
- Barath, F. T., Barrett, A. H., Copeland, J., Jones, D. E. and Lilley, A. E., 1964. Symposium on Radar and Radiometric Observations of Venus during the 1962 Conjunction: Mariner 2 microwave radiometer experiment and results. *Astronomical Journal*, 69, 49
- Barker, E. S., 1972. Detection of Molecular Oxygen in the Martian Atmosphere. *Nature*, 238, 447–448
- Barker, E. S., 1979. Detection of SO₂ in the UV spectrum of Venus. *Geophysical Research Letters*, 6, 117–120

- 734 Bates, D. R. and Nicolet, M., 1950. The Photochemistry of Atmospheric Water Vapor. *Journal of Geophysical*
735 *Research*, 55, 301–327
- 736 Baum, W. A. and Code, A. D., 1953. A photometric observation of the occultation of σ ARIETIS by Jupiter. *Astro-*
737 *nomical Journal*, 58, 108–112
- 738 Benson, J. L., Kass, D. M. and Kleinböhl, A., 2011. Mars' north polar hood as observed by the Mars Climate Sounder.
739 *Journal of Geophysical Research (Planets)*, 116, E03008
- 740 Bergstralh, J. T., 1984. Uranus and neptune. *NASA Conference Publication 2330*
- 741 Bézard, B. and de Bergh, C., 2007. Composition of the atmosphere of Venus below the clouds. *Journal of Geophysical*
742 *Research (Planets)*, 112, E04S07
- 743 Bibring, J.-P. et al, 2006. Global Mineralogical and Aqueous Mars History Derived from OMEGA/Mars Express Data.
744 *Science*, 312, 400–404
- 745 Bierson, C. J. and Zhang, X., 2020. Chemical Cycling in the Venusian Atmosphere: A Full Photochemical Model
746 From the Surface to 110 km. *Journal of Geophysical Research (Planets)*, 125, e06159
- 747 Brown, H., 1950. On the Compositions and Structures of the Planets. *Astrophysical Journal*, 111, 641
- 748 Burgdorf, M., Orton, G., van Cleve, J., Meadows, V. and Houck, J., 2006. Detection of new hydrocarbons in Uranus'
749 atmosphere by infrared spectroscopy. *Icarus*, 184, 634–637
- 750 Burton, M. R., Sawyer, G. M. and Granieri, D., 2013. Deep Carbon Emissions from Volcanoes. *Reviews in Mineralogy*
751 *and Geochemistry*, 75, 323–354
- 752 Caldeira, K. and Wickett, M. E., 2003. Oceanography: Anthropogenic carbon and ocean ph
- 753 Carr, M. H., 1996. *Water on Mars*. Oxford University Press, New York
- 754 Catling, D. C. and Claire, M. W., 2005. How earth's atmosphere evolved to an oxic state: A status report. *Earth and*
755 *Planetary Science Letters*, 237, 1–20
- 756 Cavalié, T., Venot, O., Selsis, F., Hersant, F., Hartogh, P. and Leconte, J., 2017. Thermochemistry and vertical mixing
757 in the tropospheres of Uranus and Neptune: How convection inhibition can affect the derivation of deep oxygen
758 abundances. *Icarus*, 291, 1–16. 1703.04358
- 759 Chaffin, M. S., Deighan, J., Schneider, N. M. and Stewart, A. I. F., 2017. Elevated atmospheric escape of atomic
760 hydrogen from Mars induced by high-altitude water. *Nature Geoscience*, 10, 174–178
- 761 Chamberlain, J. W. and Hunten, D. M., 1989. *Theory of Planetary Atmospheres : An Introduction to Their Physics*
762 *and Chemistry*. Number Vol. 36 in International Geophysics. Academic Press
- 763 Chambers, J. E., 2014. *Planet Formation*, volume 2. 55–72
- 764 Chapman, S., 1930. A theory of upper-atmosphere ozone. *Memoirs of the Royal Meterological Society*, 3, 103–110
- 765 Clancy, R. T., Sandor, B. J. and Moriarty-Schieven, G. H., 2004. A measurement of the 362 GHz absorption line of
766 Mars atmospheric H₂O₂. *Icarus*, 168, 116–121

- 767 Clancy, R. T., Wolff, M. J. and Christensen, P. R., 2003. Mars aerosol studies with the MGS TES emission phase
768 function observations: Optical depths, particle sizes, and ice cloud types versus latitude and solar longitude. *Journal*
769 *of Geophysical Research (Planets)*, 108, 5098
- 770 Clifford, S. M., 1993. A model for the hydrologic and climatic behavior of water on Mars. *Journal of Geophysical*
771 *Research*, 98, 10973–11016
- 772 Connes, P., Connes, J., Benedict, W. S. and Kaplan, L. D., 1967. Traces of HCl and HF in the atmosphere of Venus.
773 *Astrophysical Journal*, 147, 1230–1237
- 774 Conrath, B., Gautier, D., Hanel, R., Lindal, G. and Marten, A., 1987. The helium abundance of Uranus from Voyager
775 measurements. *Journal of Geophysical Research*, 92, 15003–15010
- 776 Conrath, B. J. and Gautier, D., 2000. Saturn helium abundance: A reanalysis of *Voyager* measurements. *Icarus*, 144,
777 124–134
- 778 Conrath, B. J., Gautier, D., Lindal, G. F., Samuelson, R. E. and Shaffer, W. A., 1991. The helium abundance of
779 Neptune from Voyager measurements. *Journal of Geophysical Research*, 96, 18907–18919
- 780 Conway, R. R., McCoy, R. P., Barth, C. A. and Lane, A. L., 1979. Iue detection of sulfur dioxide in the atmosphere
781 of Venus. *Geophysical Research Letters*, 6, 629–631
- 782 Dauphas, N., Robert, F. and Marty, B., 2000. The Late Asteroidal and Cometary Bombardment of Earth as Recorded
783 in Water Deuterium to Protium Ratio. *Icarus*, 148, 508–512
- 784 de Pater, I. and Lissauer, J. J., 2015. *Planetary Sciences*. Cambridge University Press, 2nd edition
- 785 de Pater, I. and Mitchell, D. L., 1993. Radio Observations of the planets: The importance of laboratory measurements.
786 *Journal of Geophysical Research*, 98, 5471–5490
- 787 Debras, F. and Chabrier, G., 2019. New Models of Jupiter in the Context of Juno and Galileo. *Astrophysical Journal*,
788 872, 100. 1901.05697
- 789 Demarcus, W. C., 1958. The constitution of Jupiter and Saturn. *Astronomical Journal*, 63, 2
- 790 Dobson, G. M. B. and Harrison, D. N., 1926. Measurements of the Amount of Ozone in the Earth's Atmosphere and
791 Its Relation to Other Geophysical Conditions. *Proceedings of the Royal Society of London Series A*, 110, 660–693
- 792 Domingue, D. L., Koehn, P. L., Killen, R. M., Sprague, A. L., Sarantos, M., Cheng, A. F., Bradley, E. T. and Mc-
793 Clintock, W. E., 2007. Mercury's Atmosphere: A Surface-Bounded Exosphere. *Space Science Reviews*, 131,
794 161–186
- 795 Draper, H., 1877. Photographs of the Spectra of Venus and α Lyrae. *Memorie della Societa Degli Spettroscopisti*
796 *Italiani*, 6, A2–A9
- 797 Draper, H., 1879. On photographing the spectra of the stars and planets. *Memorie della Societa Degli Spettroscopisti*
798 *Italiani*, 8, A81–A86
- 799 Duncan, M. S. and Dasgupta, R., 2017. Rise of Earth's atmospheric oxygen controlled by efficient subduction of
800 organic carbon. *Nature Geoscience*, 10, 387–392

801 Dunham, J., Theodore, 1949. Spectroscopic Observations of the Planets at Mount Wilson. In *The Atmospheres of the*
802 *Earth and Planets* (G. P. Kuiper, ed.). 288

803 Edgington, S. G., Atreya, S. K., Trafton, L. M., Caldwell, J. J., Beebe, R. F., Simon, A. A. and West, R. A., 1999.
804 Ammonia and Eddy Mixing Variations in the Upper Troposphere of Jupiter from HST Faint Object Spectrograph
805 Observations. *Icarus*, 142, 342–356

806 Edgington, S. G., Atreya, S. K., Trafton, L. M., Caldwell, J. J., Beebe, R. F., Simon, A. A., West, R. A. and Barnet,
807 C., 1998. On the Latitude Variation of Ammonia, Acetylene, and Phosphine Altitude Profiles on Jupiter from HST
808 Faint Object Spectrograph Observations. *Icarus*, 133, 192–209

809 Ehlmann, B. L., Mustard, J. F., Murchie, S. L., Bibring, J.-P., Meunier, A., Fraeman, A. A. and Langevin, Y., 2011.
810 Subsurface water and clay mineral formation during the early history of Mars. *Nature*, 479, 53–60

811 Ehlmann, B. L., Mustard, J. F., Murchie, S. L., Poulet, F., Bishop, J. L., Brown, A. J., Calvin, W. M., Clark, R. N.,
812 Des Marais, D. J., Milliken, R. E., Roach, L. H., Roush, T. L., Swayze, G. A. and Wray, J. J., 2008. Orbital
813 Identification of Carbonate-Bearing Rocks on Mars. *Science*, 322, 1828

814 Elliot, J. L., Hammel, H. B., Wasserman, L. H., Franz, O. G., McDonald, S. W., Person, M. J., Olkin, C. B., Dunham,
815 E. W., Spencer, J. R., Stansberry, J. A., Buie, M. W., Pasachoff, J. M., Babcock, B. A. and McConnochie, T. H.,
816 1998. Global warming on Triton. *Nature*, 393, 765–767

817 Encrenaz, T., Bézard, B., Greathouse, T. K., Richter, M. J., Lacy, J. H., Atreya, S. K., Wong, A. S., Lebonnois, S.,
818 Lefèvre, F. and Forget, F., 2004. Hydrogen peroxide on Mars: evidence for spatial and seasonal variations. *Icarus*,
819 170, 424–429

820 Encrenaz, T., Greathouse, T. K., Lefèvre, F. and Atreya, S. K., 2012. Hydrogen peroxide on Mars: Observations,
821 interpretation and future plans. *Planetary & Space Science*, 68, 3–17

822 Fabry, C., 1929. Le rôle des Atmosphères dans les Occultations par les Planètes. *Journal des Observateurs*, 12, 1

823 Fegley, B., 1997. NOTE: Why Pyrite Is Unstable on the Surface of Venus. *Icarus*, 128, 474–479

824 Fegley, B., Zolotov, M. Y. and Lodders, K., 1997. The Oxidation State of the Lower Atmosphere and Surface of
825 Venus. *Icarus*, 125, 416–439

826 Fegley, B., Jr., 2014. Venus. In *Meteorites, Comets, and Planets* (J. Farquhar, D. Canfield, & J. Kasting, eds.), Treatise
827 on Geochemistry, (H. D. Holland and K. K. Turekian, eds.). Elsevier Science, 2nd edition

828 Fegley, B., Jr., Gautier, D., Owen, T. and Prinn, R. G., 1991. Spectroscopy and chemistry of the atmosphere of Uranus.
829 In *Uranus* (J. T. Bergstrahl, E. D. Miner, & M. S. Matthews, eds.). Tuscon: Univ. of Arizona Press, 147–203

830 Fegley, B., Jr. and Lodders, K., 1994. Chemical models of the deep atmospheres of Jupiter and Saturn. *Icarus*, 110,
831 117–154

832 Fegley, B., Jr. and Prinn, R. G., 1985. Equilibrium and nonequilibrium chemistry of Saturn's atmosphere - Implications
833 for the observability of PH₃, N₂, CO, and GeH₄. *Astrophysical Journal*, 299, 1067–1078

834 Fegley, B., Jr. and Prinn, R. G., 1986. Chemical models of the deep atmosphere of Uranus. *Astrophysical Journal*,
835 307, 852–865

- 836 Fegley, B., Jr. and Prinn, R. G., 1989. *The Formation and Evolution of Planetary Systems*. Cambridge: Cambridge
837 Univ. Press, 171–211
- 838 Formisano, V., Atreya, S., Encrenaz, T., Ignatiev, N. and Giuranna, M., 2004. Detection of Methane in the Atmosphere
839 of Mars. *Science*, 306, 1758–1761
- 840 Fortney, J. J. and Hubbard, W. B., 2003. Phase separation in giant planets: inhomogeneous evolution of Saturn. *Icarus*,
841 164, 228–243
- 842 Fowler, A. and Strutt, R. J., 1917. Absorption Bands of Atmospheric Ozone in the Spectra of Sun and Stars. *Proceed-*
843 *ings of the Royal Society of London Series A*, 93, 577–586
- 844 Franz, H. B., Trainer, M. G., Malespin, C. A., Mahaffy, P. R., Atreya, S. K., Becker, R. H., Benna, M., Conrad, P. G.,
845 Eigenbrode, J. L., Freissinet, C., Manning, H. L. K., Prats, B. D., Raaen, E. and Wong, M. H., 2017. Initial SAM
846 calibration gas experiments on Mars: Quadrupole mass spectrometer results and implications. *Planetary & Space*
847 *Science*, 138, 44–54
- 848 Frederick, J. E., 2008. *Principles of Atmospheric Science*. Reading, Massachusetts: Jones & Bartlett Learning
- 849 Friedlingstein, P., O’Sullivan, M., Jones, M. W. et al, 2020. Global Carbon Budget 2020. *Earth System Science Data*,
850 12, 3269–3340
- 851 Galloway, J. N., Leach, A. M., Bleeker, A. and Erisman, J. W., 2013. A chronology of human understanding of the
852 nitrogen cycle. *Philosophical Transactions of the Royal Society B: Biological Sciences*, 368, 20130120
- 853 Gautier, D., Conrath, B. J., Owen, T., de Pater, I. and Atreya, S. K., 1995. The troposphere of Neptune. In *Neptune*
854 *and Triton*. 547–611
- 855 Gierasch, P. J., Ingersoll, A. P., Banfield, D., Ewald, S. P., Helfenstein, P., Simon-Miller, A., Vasavada, A., Breneman,
856 H. H., Senske, D. A. and A4 Galileo Imaging Team, 2000. Observation of moist convection in Jupiter’s atmosphere.
857 *Nature*, 403, 628–630
- 858 Giles, R. S., Fletcher, L. N. and Irwin, P. G. J., 2017a. Latitudinal variability in Jupiter’s tropospheric disequilibrium
859 species: GeH₄, AsH₃ and PH₃. *Icarus*, 289, 254–269. 1610.09073
- 860 Gladstone, G. R., Allen, M. and Yung, Y. L., 1996. Hydrocarbon photochemistry in the upper atmosphere of Jupiter.
861 *Icarus*, 119, 1–52
- 862 Grandjean, J. and Goody, R. M., 1955. The Concentration of Carbon Dioxide in the Atmosphere of Mars. *Astrophys-*
863 *ical Journal*, 121, 548
- 864 Grassi, D., Adriani, A., Mura, A., Atreya, S. K., Fletcher, L. N., Lunine, J. I., Orton, G. S., Bolton, S., Plainaki, C.,
865 Sindoni, G., Altieri, F., Cicchetti, A., Dinelli, B. M., Filacchione, G., Migliorini, A., Moriconi, M. L., Noschese,
866 R., Olivieri, A., Piccioni, G., Sordini, R., Stefani, S., Tosi, F. and Turrini, D., 2020. On the Spatial Distribution
867 of Minor Species in Jupiter’s Troposphere as Inferred From Juno JIRAM Data. *Journal of Geophysical Research*
868 *(Planets)*, 125, e06206
- 869 Guillot, T., 1999. Interior of giant planets inside and outside the solar system. *Science*, 286, 72–77

- Guillot, T., Stevenson, D. J., Hubbard, W. B. and Saumon, D., 2004. The interior of Jupiter. In *Jupiter: The Planet, Satellites and Magnetosphere* (F. Bagenal, T. E. Dowling, & W. B. McKinnon, eds.). Cambridge: Cambridge Univ. Press, 35–57
- Halliday, A. N., 2013. The origins of volatiles in the terrestrial planets. *Geochimica et Cosmochimica Acta*, 105, 146–171
- Hartley, W. N., 1881. Xxi. on the absorption of solar rays by atmospheric ozone. *J Chem Soc, Trans*, 39, 111–128
- Hecht, M. H., Kounaves, S. P., Quinn, R. C., West, S. J., Young, S. M. M., Ming, D. W., Catling, D. C., Clark, B. C., Boynton, W. V., Hoffman, J., DeFlores, L. P., Gospodinova, K., Kapit, J. and Smith, P. H., 2009. Detection of Perchlorate and the Soluble Chemistry of Martian Soil at the Phoenix Lander Site. *Science*, 325, 64
- Herschel, W., 1784. On the Remarkable Appearances at the Polar Regions of the Planet Mars, the Inclination of Its Axis, the Position of Its Poles, and Its Spheroidal Figure; With a Few Hints Relating to Its Real Diameter and Atmosphere. By William Herschel, Esq. F. R. S. *Philosophical Transactions of the Royal Society of London Series I*, 74, 233–273
- Herzberg, G., 1952. Spectroscopic evidence of molecular hydrogen in the atmospheres of Uranus and Neptune. *Astrophysical Journal*, 115, 337–340
- Hess, S. L., 1948. A Meteorological Approach to the Question of Water Vapor on Mars and the Mass of the Martian Atmosphere. *Publications of the Astronomical Society of the Pacific*, 60, 289
- Hess, S. L., Henry, R. M., Leovy, C. B., Ryan, J. A. and Tillman, J. E., 1977. Meteorological results from the surface of Mars: Viking 1 and 2. *Journal of Geophysical Research*, 82, 4559–4574
- Hess, S. L., Ryan, J. A., Tillman, J. E., Henry, R. M. and Leovy, C. B., 1980. The annual cycle of pressure on Mars measured by Viking Landers 1 and 2. *Geophysical Research Letters*, 7, 197–200
- Holstein-Rathlou, C., Maue, A. and Withers, P., 2016. Atmospheric studies from the Mars Science Laboratory Entry, Descent and Landing atmospheric structure reconstruction. *Planetary & Space Science*, 120, 15–23
- Hörst, S. M., 2017. Titan’s atmosphere and climate. *Journal of Geophysical Research (Planets)*, 122, 432–482. 1702.08611
- Hubbard, W. B., 1968. Thermal structure of Jupiter. *Astrophysical Journal*, 152, 745–754
- Hubbard, W. B., 1969. Thermal models of Jupiter and Saturn. *Astrophysical Journal*, 155, 333–+
- Hubbard, W. B., Podolak, M. and Stevenson, D. J., 1995. The interior of Neptune. In *Neptune and Triton*. 109–138
- Huggins, W., 1867. On the Spectrum of Mars, with some Remarks on the Colour of that Planet. *Monthly Notices of the Royal Astronomical Society*, 27, 178
- Huggins, W., 1876. Note on the Photographic Spectra of Stars. *Proceedings of the Royal Society of London Series I*, 25, 445–446
- Ingersoll, A. P., Gierasch, P. J., Banfield, D., Vasavada, A. R. and A3 *Galileo* Imaging Team, 2000. Moist convection as an energy source for the large-scale motions in Jupiter’s atmosphere. *Nature*, 403, 630–632

- 904 Irwin, P. G. J., Toledo, D., Braude, A. S., Bacon, R., Weilbacher, P. M., Teanby, N. A., Fletcher, L. N. and Orton,
905 G. S., 2019. Latitudinal variation in the abundance of methane (CH₄) above the clouds in Neptune's atmosphere
906 from VLT/MUSE Narrow Field Mode Observations. *Icarus*, 331, 69–82. 1905.03516
- 907 Jakosky, B. M. and Phillips, R. J., 2001. Mars' volatile and climate history. *Nature*, 412, 237–244
- 908 Jakosky, B. M., Slipski, M., Benna, M., Mahaffy, P., Elrod, M., Yelle, R., Stone, S. and Alsaeed, N., 2017. Mars'
909 atmospheric history derived from upper-atmosphere measurements of ³⁸Ar/³⁶Ar. *Science*, 355, 1408–1410
- 910 Jakosky, B. M. et al, 2015. The Mars Atmosphere and Volatile Evolution (MAVEN) Mission. *Space Science Reviews*,
911 195, 3–48
- 912 Jakosky, B. M. et al, 2018. Loss of the Martian atmosphere to space: Present-day loss rates determined from MAVEN
913 observations and integrated loss through time. *Icarus*, 315, 146–157
- 914 Jeffreys, H., 1924. On the internal constitution of Jupiter and Saturn. *Monthly Notices of the Royal Astronomical*
915 *Society*, 84, 534
- 916 Johnson, B. and Goldblatt, C., 2015. The nitrogen budget of earth. *Earth-Science Reviews*, 148, 150–173
- 917 Kaplan, L. D., Münch, G. and Spinrad, H., 1964. An Analysis of the Spectrum of Mars. *Astrophysical Journal*, 139, 1
- 918 Kaye, J. A. and Strobel, D. F., 1983. Phosphine photochemistry in Saturn's atmosphere. *Geophysical Research Letters*,
919 10, 957–960
- 920 Kaye, J. A. and Strobel, D. F., 1984. Phosphine photochemistry in the atmosphere of Saturn. *Icarus*, 59, 314–335
- 921 Keeling, R. F. and Keeling, C., 2017. Atmospheric Monthly In Situ CO₂ Data - Mauna Loa Observatory, Hawaii. In
922 *Scripps CO₂ Program Data, UC San Diego Library Digital Collections*.
- 923 Kelly, N. J., Boynton, W. V., Kerry, K., Hamara, D., Janes, D., Reedy, R. C., Kim, K. J. and Haberle, R. M., 2006. Sea-
924 sonal polar carbon dioxide frost on Mars: CO₂ mass and columnar thickness distribution. *Journal of Geophysical*
925 *Research (Planets)*, 111, E03S07
- 926 Killen, R., Cremonese, G., Lammer, H., Orsini, S., Potter, A. E., Sprague, A. L., Wurz, P., Khodachenko, M. L.,
927 Lichtenegger, H. I. M., Milillo, A. and Mura, A., 2007. Processes that Promote and Deplete the Exosphere of
928 Mercury. *Space Science Reviews*, 132, 433–509
- 929 Killen, R. M. and Ip, W.-H., 1999. The surface-bounded atmospheres of Mercury and the Moon. *Reviews of Geo-*
930 *physics*, 37, 361–406
- 931 Kirchhoff, G., 1860. Ueber das Verhältniss zwischen dem Emissionsvermögen und dem Absorptionsvermögen der
932 Körper für Wärme und Licht. *Annalen der Physik*, 185, 275–301
- 933 Kirchhoff, G. and Bunsen, R., 1860. Chemische Analyse durch Spectralbeobachtungen. *Annalen der Physik*, 186,
934 161–189
- 935 Kolodner, M. A. and Steffes, P. G., 1998. The Microwave Absorption and Abundance of Sulfuric Acid Vapor in the
936 Venus Atmosphere Based on New Laboratory Measurements. *Icarus*, 132, 151–169

- 937 Korablev, O., Avandaele, A. C., Montmessin, F. et al, 2019. No detection of methane on Mars from early ExoMars
938 Trace Gas Orbiter observations. *Nature*, 568, 517–520
- 939 Krasnopolsky, V. A., 1993. Photochemistry of the Martian Atmosphere (Mean Conditions). *Icarus*, 101, 313–332
- 940 Krasnopolsky, V. A., 2006. Photochemistry of the martian atmosphere: Seasonal, latitudinal, and diurnal variations.
941 *Icarus*, 185, 153–170
- 942 Krasnopolsky, V. A., 2012. A photochemical model for the Venus atmosphere at 47–112 km. *Icarus*, 218, 230–246
- 943 Krasnopolsky, V. A. and Feldman, P. D., 2001. Detection of Molecular Hydrogen in the Atmosphere of Mars. *Science*,
944 294, 1914–1917
- 945 Kuiper, G. P., 1952. *The atmospheres of the earth and planets*. University of Chicago Press, revised edition
- 946 Lammer, H., Brasser, R., Johansen, A., Scherf, M. and Leitzinger, M., 2021. Formation of Venus, Earth and Mars:
947 Constrained by Isotopes. *Space Science Reviews*, 217, 7. 2102.06173
- 948 Lary, D. J., 1997. Catalytic destruction of stratospheric ozone. *Journal of Geophysical Research*, 102, 21,515–21,526
- 949 Lefèvre, F., Bertaux, J.-L., Clancy, R. T., Encrenaz, T., Fast, K., Forget, F., Lebonnois, S., Montmessin, F. and Perrier,
950 S., 2008. Heterogeneous chemistry in the atmosphere of Mars. *Nature*, 454, 971–975
- 951 Lellouch, E., 2005. Io's Atmosphere and Surface-Atmosphere Interactions. *Space Science Reviews*, 116, 211–224
- 952 Lellouch, E., de Bergh, C., Sicardy, B., Ferron, S. and Käufl, H. U., 2010. Detection of CO in Triton's atmosphere
953 and the nature of surface-atmosphere interactions. *Astronomy & Astrophysics*, 512, L8. 1003.2866
- 954 Leovy, C. B., Briggs, G. A. and Smith, B. A., 1973. Mars Atmosphere during the Mariner 9 Extended Mission:
955 Television Results. *Journal of Geophysical Research*, 78, 4252–4266
- 956 Lewis, J. S., 1969. The clouds of Jupiter and the $\text{NH}_3\text{-H}_2\text{O}$ and $\text{NH}_3\text{-H}_2\text{S}$ systems. *Icarus*, 10, 365–378
- 957 Lewis, J. S. and Prinn, R. G., 1970. Jupiter's clouds: structure and composition. *Science*, 169, 472–473
- 958 Li, C., Ingersoll, A., Bolton, S., Levin, S., Janssen, M., Atreya, S., Lunine, J., Steffes, P., Brown, S., Guillot, T.,
959 Allison, M., Arballo, J., Bellotti, A., Adumitroaie, V., Gulkis, S., Hodges, A., Li, L., Misra, S., Orton, G., Oyafuso,
960 F., Santos-Costa, D., Waite, H. and Zhang, Z., 2020. The water abundance in jupiter's equatorial zone. *Nature*
961 *Astron*
- 962 Li, C., Ingersoll, A., Janssen, M., Levin, S., Bolton, S., Adumitroaie, V., Allison, M., Arballo, J., Bellotti, A., Brown,
963 S., Ewald, S., Jewell, L., Misra, S., Orton, G., Oyafuso, F., Steffes, P. and Williamson, R., 2017. The distribution
964 of ammonia on Jupiter from a preliminary inversion of Juno microwave radiometer data. *Geophysical Research*
965 *Letters*, 44, 5317–5325
- 966 Lilley, A. E., 1961. The Temperature of Venus. *Astronomical Journal*, 70, 290
- 967 Limaye, S. S., Grassi, D., Mahieux, A., Migliorini, A., Tellmann, S. and Titov, D., 2018. Venus Atmospheric Thermal
968 Structure and Radiative Balance. *Space Science Reviews*, 214, 102

- 969 Lindal, G. F., 1992. The atmosphere of Neptune - an analysis of radio occultation data acquired with Voyager 2.
970 *Astronomical Journal*, 103, 967–982
- 971 Lindal, G. F., Sweetnam, D. N. and Eshleman, V. R., 1985. The atmosphere of Saturn - an analysis of the *Voyager*
972 radio occultation measurements. *Astronomical Journal*, 90, 1136–1146
- 973 Lissauer, J. J., 1993. Planet formation. *Annual Review of Astronomy & Astrophysics*, 31, 129–174
- 974 Lodders, K., 2004. Jupiter formed with more tar than ice. *Astrophysical Journal*, 611, 587–597
- 975 Lodders, K., 2020. Solar Elemental Abundances. *Oxford Research Encyclopedia of Planetary Science*
- 976 Lodders, K. and Fegley, B., 2011. *Chemistry of the Solar System*. Cambridge: Royal Society of Chemistry
- 977 Lodders, K. and Fegley, B., Jr., 1994. The origin of carbon monoxide in Neptunes’s atmosphere. *Icarus*, 112, 368–375
- 978 Lodders, K. and Fegley, B., Jr., 1998. *The Planetary Scientist’s Companion*. New York: Oxford Univ. Press
- 979 Lodders, K. and Fegley, B., Jr., 2002. Atmospheric chemistry in giant planets, brown dwarfs, and low-mass dwarf
980 stars. I. Carbon, nitrogen, and oxygen. *Icarus*, 155, 393–424
- 981 Lodders, K. and Fegley, B., Jr., 2006. Chemistry of Low Mass Substellar Objects. In *Astrophysics Update 2* (J. W.
982 Mason, ed.). Berlin: Springer Verlag, 1–28
- 983 Low, F. J., 1966. Observations of Venus, Jupiter, and Saturn at $\lambda 20\mu$. *Astronomical Journal*, 71, 391–+
- 984 Lunine, J. I., Coradini, A., Gautier, D., Owen, T. C. and Wuchterl, G., 2004. The origin of Jupiter. In *Jupiter: The*
985 *Planet, Satellites and Magnetosphere* (F. Bagenal, T. E. Dowling, & W. B. McKinnon, eds.). Cambridge: Cam-
986 bridge Univ. Press, 19–34
- 987 Lyons, T. W., Reinhard, C. T. and Planavsky, N. J., 2014. The rise of oxygen in Earth’s early ocean and atmosphere.
988 *Nature*, 506, 307–315
- 989 Määttänen, A. and F., M., 2021. Clouds in the Martian Atmosphere. *Oxford Research Encyclopedia of Planetary*
990 *Science*
- 991 Mahaffy, P. R., Niemann, H. B., Alpert, A., Atreya, S. K., Demick, J., Donahue, T. M., Harpold, D. N. and Owen,
992 T. C., 2000. Noble gas abundance and isotope ratios in the atmosphere of Jupiter from the *Galileo* Probe Mass
993 Spectrometer. *Journal of Geophysical Research*, 105, 15061–15072
- 994 Mahaffy, P. R. et al, 2013. Abundance and Isotopic Composition of Gases in the Martian Atmosphere from the
995 Curiosity Rover. *Science*, 341, 263–266
- 996 Marcq, E., Encrenaz, T., Bézard, B. and Birlan, M., 2006. Remote sensing of Venus’ lower atmosphere from ground-
997 based IR spectroscopy: Latitudinal and vertical distribution of minor species. *Planetary & Space Science*, 54,
998 1360–1370
- 999 Marcq, E., Mills, F. P., Parkinson, C. D. and Vandaale, A. C., 2018. Composition and Chemistry of the Neutral
1000 Atmosphere of Venus. *Space Science Reviews*, 214, 10
- 1001 Marley, M. S. and Fortney, J. J., 2007. *Interiors of the Giant Planets*. 403–418

- 1002 Marov, M. Y., 2004. Mikhail Iomonosov and the discovery of the atmosphere of Venus during the 1761 transit.
1003 *Proceedings of the International Astronomical Union*, 2004, 209–219
- 1004 Marty, B., 2012. The origins and concentrations of water, carbon, nitrogen and noble gases on Earth. *Earth and*
1005 *Planetary Science Letters*, 313, 56–66. 1405.6336
- 1006 Mazor, E., Heymann, D. and Anders, E., 1970. Noble gases in carbonaceous chondrites. *Geochimica et Cosmochimica*
1007 *Acta*, 34, 781–824
- 1008 McElroy, M. B. and Donahue, T. M., 1972. Stability of the Martian Atmosphere. *Science*, 177, 986–988
- 1009 McGrath, M. A., Lellouch, E., Strobel, D. F., Feldman, P. D. and Johnson, R. E., 2004. *Satellite atmospheres*, volume 1.
1010 457–483
- 1011 Merkel, A. W., Cassidy, T. A., Vervack, R. J., McClintock, W. E., Sarantos, M., Burger, M. H. and Killen, R. M.,
1012 2017. Seasonal variations of Mercury’s magnesium dayside exosphere from MESSENGER observations. *Icarus*,
1013 281, 46–54
- 1014 Mills, F. P., Esposito, L. W. and Yung, Y. L., 2007. Atmospheric composition, chemistry, and clouds. *Washington DC*
1015 *American Geophysical Union Geophysical Monograph Series*, 176, 73–100
- 1016 Mills, F. P., Marcq, E., Yung, Y., Parkinson, C. D., Jessup, K. L. and Vandaele, A. C., 2019. Atmospheric Chemistry
1017 on Venus: An Overview of Unresolved Issues. In *Lunar and Planetary Science Conference*, Lunar and Planetary
1018 Science Conference. 2374
- 1019 Montmessin, F., Bertaux, J.-L., Quémerais, E., Korabiev, O., Rannou, P., Forget, F., Perrier, S., Fussen, D., Lebonnois,
1020 S., Réberac, A. and Dimarellis, E., 2006. Subvisible CO₂ ice clouds detected in the mesosphere of Mars. *Icarus*,
1021 183, 403–410
- 1022 Morbidelli, A., Chambers, J., Lunine, J. I., Petit, J. M., Robert, F., Valsecchi, G. B. and Cyr, K. E., 2000. Source
1023 regions and time scales for the delivery of water to Earth. *Meteoritics and Planetary Science*, 35, 1309–1320
- 1024 Moroz, V. I. and Zasova, L. V., 1997. VIRA-2: a review of inputs for updating the Venus International Reference
1025 Atmosphere. *Advances in Space Research*, 19, 1191–1201
- 1026 Moses, J. I., Allen, M. and Yung, Y. L., 1992. Hydrocarbon nucleation and aerosol formation in Neptune’s atmosphere.
1027 *Icarus*, 99, 318–346
- 1028 Moses, J. I., Bézard, B., Lellouch, E., Gladstone, G. R., Feuchtgruber, H. and Allen, M., 2000. Photochemistry of
1029 Saturn’s atmosphere. I. Hydrocarbon chemistry and comparisons with ISO observations. *Icarus*, 143, 244–298
- 1030 Moses, J. I., Cavalie, T., Fletcher, L. N. and Roman, M. T., 2020. Atmospheric chemistry on Uranus and Neptune.
1031 *arXiv e-prints*, arXiv:2006.11367. 2006.11367
- 1032 Moses, J. I., Fletcher, L. N., Greathouse, T. K., Orton, G. S. and Hue, V., 2018. Seasonal stratospheric photochemistry
1033 on Uranus and Neptune. *Icarus*, 307, 124–145. 1803.10338
- 1034 Moses, J. I., Fouchet, T., Bézard, B., Gladstone, G. R., Lellouch, E. and Feuchtgruber, H., 2005. Photochemistry and
1035 diffusion in Jupiter’s stratosphere: Constraints from ISO observations and comparisons with other giant planets.
1036 *Journal of Geophysical Research (Planets)*, 110, 8001

- 1037 Moses, J. I., Rages, K. and Pollack, J. B., 1995. An analysis of Neptune's stratospheric haze using high-phase-angle
1038 voyager images. *Icarus*, 113, 232–266
- 1039 Mueller, R. F., 1963. Chemistry and Petrology of Venus: Preliminary Deductions. *Science*, 141, 1046–1047
- 1040 Mueller, R. F., 1964. A Chemical Model for the Lower Atmosphere of Venus. *Icarus*, 3, 285–298
- 1041 Mumma, M. J., Villanueva, G. L., Novak, R. E., Hewagama, T., Bonev, B. P., DiSanti, M. A., Mandell, A. M. and
1042 Smith, M. D., 2009. Strong Release of Methane on Mars in Northern Summer 2003. *Science*, 323, 1041
- 1043 Nair, H., Allen, M., Anbar, A. D., Yung, Y. L. and Clancy, R. T., 1994. A Photochemical Model of the Martian
1044 Atmosphere. *Icarus*, 111, 124–150
- 1045 Navarro-González, R., Vargas, E., de la Rosa, J., Raga, A. C. and McKay, C. P., 2010. Reanalysis of the Viking
1046 results suggests perchlorate and organics at midlatitudes on Mars. *Journal of Geophysical Research (Planets)*, 115,
1047 E12010
- 1048 NOAA/NASA/USAF, 1976. U.S. Standard Atmosphere, 1976. *NASA-TM-X-74335, NOAA-S/T-76-1562*
- 1049 Norrish, R. G. W. and Wayne, R. P., 1965a. The Photolysis of Ozone by Ultraviolet Radiation. I. The Photolysis of
1050 Pure, Dry Ozone. *Proceedings of the Royal Society of London Series A*, 288, 200–211
- 1051 Norrish, R. G. W. and Wayne, R. P., 1965b. The Photolysis of Ozone by Ultraviolet Radiation. II. The Photolysis of
1052 Ozone Mixed With Certain Hydrogen-Containing Substances. *Proceedings of the Royal Society of London Series*
1053 *A*, 288, 361–370
- 1054 O'Brien, D. P., Izidoro, A., Jacobson, S. A., Raymond, S. N. and Rubie, D. C., 2018. The Delivery of Water During
1055 Terrestrial Planet Formation. *Space Science Reviews*, 214, 47. 1801.05456
- 1056 Oyama, V. I. and Berdahl, B. J., 1977. The Viking gas exchange experiment results from Chryse and Utopia surface
1057 samples. *Journal of Geophysical Research*, 82, 4669–4676
- 1058 Pearl, J. C., Conrath, B. J., Hanel, R. A., Pirraglia, J. A. and Coustenis, A., 1990. The albedo, effective temperature,
1059 and energy balance of Uranus, as determined from Voyager IRIS data. *Icarus*, 84, 12–28
- 1060 Pearl, J. C., Smith, M. D., Conrath, B. J., Bandfield, J. L. and Christensen, P. R., 2001. Observations of Martian
1061 ice clouds by the Mars Global Surveyor Thermal Emission Spectrometer: The first Martian year. *Journal of*
1062 *Geophysical Research*, 106, 12325–12338
- 1063 Peebles, P. J. E., 1964. The structure and composition of Jupiter and Saturn. *Astrophysical Journal*, 140, 328–+
- 1064 Pepin, R. O., 1991. On the origin and early evolution of terrestrial planet atmospheres and meteoritic volatiles. *Icarus*,
1065 92, 2–79
- 1066 Pepin, R. O., 2006. Atmospheres on the terrestrial planets: Clues to origin and evolution. *Earth and Planetary Science*
1067 *Letters*, 252, 1–14
- 1068 Plank, T. and Manning, C. E., 2019. Subducting carbon. *Nature*, 574, 343–352
- 1069 Podolak, M., Hubbard, W. B. and Stevenson, D. J., 1991. *Models of Uranus' interior and magnetic field*. 29–61

- 1070 Pollack, J. B. and Black, D. C., 1982. Noble gases in planetary atmospheres: Implications for the origin and evolution
1071 of atmospheres. *Icarus*, 51, 169–198
- 1072 Pollack, J. B., Colburn, D., Kahn, R., Hunter, J., van Camp, W., Carlston, C. E. and Wolf, M. R., 1977. Properties of
1073 aerosols in the Martian atmosphere, as inferred from Viking lander imaging data. *Journal of Geophysical Research*,
1074 82, 4479–4496
- 1075 Pollack, J. B., Kasting, J. F., Richardson, S. M. and Poliakoff, K., 1987. The case for a wet, warm climate on early
1076 Mars. *Icarus*, 71, 203–224
- 1077 Potter, A. and Morgan, T., 1985. Discovery of Sodium in the Atmosphere of Mercury. *Science*, 229, 651–653
- 1078 Potter, A. E. and Morgan, T. H., 1986. Potassium in the atmosphere of Mercury. *Icarus*, 67, 336–340
- 1079 Prinn, R. G., 1971. Photochemistry of HCl and other minor constituents in the atmosphere of Venus. *Journal of*
1080 *Atmospheric Sciences*, 28, 1058–1068
- 1081 Prinn, R. G. and Barshay, S. S., 1977. Carbon monoxide on Jupiter and implications for atmospheric convection.
1082 *Science*, 198, 1031–1034
- 1083 Prinn, R. G. and Lewis, J. S., 1975. Phosphine on Jupiter and Implications for the Great Red Spot. *Science*, 190,
1084 274–276
- 1085 Ramsey, W. H., 1951. On the constitutions of the major planets. *Monthly Notices of the Royal Astronomical Society*,
1086 111, 427
- 1087 Read, P. L., Barstow, J., Charnay, B., Chelvaniththilan, S., Irwin, P. G. J., Knight, S., Lebonnois, S., Lewis, S. R.,
1088 Mendonça, J. and Montabone, L., 2016. Global energy budgets and ‘Trenberth diagrams’ for the climates of
1089 terrestrial and gas giant planets. *Quarterly Journal of the Royal Meteorological Society*, 142, 703–720
- 1090 Romani, P. N. and Atreya, S. K., 1988. Methane photochemistry and haze production on Neptune. *Icarus*, 74, 424–445
- 1091 Roulston, M. S. and Stevenson, D. J., 1995. Prediction of neon depletion in Jupiter’s atmosphere. *EOS Transactions*,
1092 76, 343
- 1093 Sano, Y., Takahata, N., Nishio, Y., Fischer, T. P. and Williams, S. N., 2001. Volcanic flux of nitrogen from the Earth.
1094 *Chemical Geology*, 171, 263–271
- 1095 Scheller, E. L., Ehlmann, B. L., Hu, R., Adams, D. J. and Yung, Y. L., 2021. Long-term drying of Mars by sequestration
1096 of ocean-scale volumes of water in the crust. *Science*, 372, 56–62
- 1097 Schofield, J. T., Barnes, J. R., Crisp, D., Haberle, R. M., Larsen, S., Magalhães, J. A., Murphy, J. R., Seiff, A.
1098 and Wilson, G., 1997. The mars pathfinder atmospheric structure investigation/meteorology (asi/met) experiment.
1099 *Science*, 278, 1752–1758. <https://science.sciencemag.org/content/278/5344/1752.full.pdf>
- 1100 Seiff, A. and Kirk, D. B., 1977. Structure of the atmosphere of Mars in summer at mid-latitudes. *Journal of Geophys-*
1101 *ical Research*, 82, 4364–4378
- 1102 Seiff, A., Kirk, D. B., Knight, T. C. D., Young, R. E., Mihalov, J. D., Young, L. A., Milos, F. S., Schubert, G.,
1103 Blanchard, R. C. and Atkinson, D., 1998. Thermal structure of Jupiter’s atmosphere near the edge of a 5- μ m hot
1104 spot in the north equatorial belt. *Journal of Geophysical Research*, 103, 22857–22890

- 1105 Seiff, A., Schofield, J. T., Kliore, A. J., Taylor, F. W., Limaye, S. S., Revercomb, H. E., Sromovsky, L. A.,
 1106 Kerzhanovich, V. V., Moroz, V. I. and Marov, M. Y., 1985. Models of the structure of the atmosphere of Venus
 1107 from the surface to 100 kilometers altitude. *Advances in Space Research*, 5, 3–58
- 1108 Sill, G. T., 1972. Sulfuric acid in the Venus clouds. *Communications of the Lunar and Planetary Laboratory*, 9,
 1109 191–198
- 1110 Slipher, V. M., 1904. The Lowell Spectrograph. *Astrophysical Journal*, 20, 1
- 1111 Smith, B. A. et al, 1989. Voyager 2 at Neptune: Imaging Science Results. *Science*, 246, 1422–1449
- 1112 Spencer, J. R., Stansberry, J. A., Trafton, L. M., Young, E. F., Binzel, R. P. and Croft, S. K., 1997. *Volatile Transport,*
 1113 *Seasonal Cycles, and Atmospheric Dynamics on Pluto*. 435
- 1114 Spiga, A., 2019. The Planetary Boundary Layer of Mars. *Oxford Research Encyclopedia of Planetary Science*, 130
- 1115 Stevenson, D. J., 1982. Interiors of the Giant Planets. *Annual Review of Earth and Planetary Sciences*, 10, 257
- 1116 Stewart, A. I., Anderson, D. E., Esposito, L. W. and Barth, C. A., 1979. Ultraviolet Spectroscopy of Venus: Initial
 1117 Results from the Pioneer Venus Orbiter. *Science*, 203, 777–779
- 1118 Stone, E. C. and Miner, E. D., 1989. The Voyager 2 Encounter with the Neptunian System. *Science*, 246, 1417–1421
- 1119 Summers, M. E. and Strobel, D. F., 1989. Photochemistry of the Atmosphere of Uranus. *Astrophysical Journal*, 346,
 1120 495
- 1121 Summers, M. E., Strobel, D. F. and Gladstone, G. R., 1997. *Chemical Models of Pluto's Atmosphere*. 391
- 1122 Taylor, F. W., Atreya, S. K., Encrenaz, T., Hunten, D. M., Irwin, P. G. J. and Owen, T. C., 2004. The composition
 1123 of the atmosphere of Jupiter. In *Jupiter: The Planet, Satellites and Magnetosphere* (F. Bagenal, T. E. Dowling, &
 1124 W. B. McKinnon, eds.). Cambridge: Cambridge Univ. Press, 59–78
- 1125 Teanby, N. A., Irwin, P. G. J. and Moses, J. I., 2019. Neptune's carbon monoxide profile and phosphine upper limits
 1126 from Herschel/SPIRE: Implications for interior structure and formation. *Icarus*, 319, 86–98
- 1127 Thomas, N. C., 1991. The early history of spectroscopy. *Journal of Chemical Education*, 68, 631. <https://doi.org/10.1021/ed068p631>
- 1129 Titov, D. V., Ignatiev, N. I., McGouldrick, K., Wilquet, V. and Wilson, C. F., 2018. Clouds and Hazes of Venus. *Space*
 1130 *Science Reviews*, 214, 126
- 1131 Trafton, L., 1981. The atmospheres of the outer planets and satellites. *Reviews of Geophysics and Space Physics*, 19,
 1132 43–89
- 1133 Trainer, M. G., Wong, M. H., McConnochie, T. H., Franz, H. B., Atreya, S. K., Conrad, P. G., Lefèvre, F., Mahaffy,
 1134 P. R., Malespin, C. A., Manning, H. L. K., Martín-Torres, J., Martínez, G. M., McKay, C. P., Navarro-González, R.,
 1135 Vicente-Retortillo, Á., Webster, C. R. and Zorzano, M.-P., 2019. Seasonal Variations in Atmospheric Composition
 1136 as Measured in Gale Crater, Mars. *Journal of Geophysical Research (Planets)*, 124, 3000–3024
- 1137 Trieloff, M., 2017. Noble Gases. *Oxford Research Encyclopedia of Planetary Science*, 30

- 1138 Urey, H. C., 1951. The origin and development of the earth and other terrestrial planets. *Geochimica et Cosmochimica*
1139 *Acta*, 1, 209–277
- 1140 Vandaale, A. C., 2020. Composition and Chemistry of the Neutral Atmosphere of Venus. *Oxford Research Encyclo-*
1141 *pedia of Planetary Science*
- 1142 Vervack, R. J., McClintock, W. E., Killen, R. M., Sprague, A. L., Anderson, B. J., Burger, M. H., Bradley, E. T.,
1143 Mouawad, N., Solomon, S. C. and Izenberg, N. R., 2010. Mercury’s Complex Exosphere: Results from MESSEN-
1144 GER’s Third Flyby. *Science*, 329, 672
- 1145 Villanueva, G. L., Mumma, M. J., Novak, R. E., Radeva, Y. L., Käufl, H. U., Smette, A., Tokunaga, A., Khayat, A.,
1146 Encrenaz, T. and Hartogh, P., 2013. A sensitive search for organics (CH₄, CH₃OH, H₂CO, C₂H₆, C₂H₂, C₂H₄),
1147 hydroperoxyl (HO₂), nitrogen compounds (N₂O, NH₃, HCN) and chlorine species (HCl, CH₃Cl) on Mars using
1148 ground-based high-resolution infrared spectroscopy. *Icarus*, 223, 11–27
- 1149 Visscher, C., 2020. Mapping Jupiter’s Mischief. *Journal of Geophysical Research (Planets)*, 125, e06526
- 1150 Visscher, C. and Fegley, B., Jr., 2005. Chemical constraints on the water and total oxygen abundances in the deep
1151 atmosphere of Saturn. *Astrophysical Journal*, 623, 1221–1227
- 1152 Visscher, C., Lodders, K. and Fegley, B., Jr., 2006. Atmospheric Chemistry in Giant Planets, Brown Dwarfs, and
1153 Low-Mass Dwarf Stars. II. Sulfur and Phosphorus. *Astrophysical Journal*, 648, 1181–1195. astro-ph/0511136
- 1154 Visscher, C., Lodders, K. and Fegley, B., Jr., 2010a. Atmospheric Chemistry in Giant Planets, Brown Dwarfs, and
1155 Low-mass Dwarf Stars. III. Iron, Magnesium, and Silicon. *Astrophysical Journal*, 716, 1060–1075. 1001.3639
- 1156 Visscher, C. and Moses, J. I., 2011. Quenching of Carbon Monoxide and Methane in the Atmospheres of Cool Brown
1157 Dwarfs and Hot Jupiters. *Astrophysical Journal*, 738, 72
- 1158 Visscher, C., Moses, J. I. and Saslow, S. A., 2010b. The Deep Water Abundance on Jupiter: New Constraints from
1159 Thermochemical Kinetics and Diffusion Modeling. *Icarus*, 209, 602–615
- 1160 Visscher, C., Sperier, A. D., Moses, J. I. and Keane, T. C., 2009. Phosphine and Ammonia Photochemistry in Jupiter’s
1161 Troposphere. In *Lunar and Planetary Institute Science Conference Abstracts*, volume 40. 1201
- 1162 von Zahn, U., Kumar, S., Niemann, H. and Prinn, R., 1983. *Composition of the Venus atmosphere*. 299
- 1163 Wahl, S. M., Hubbard, W. B., Militzer, B., Guillot, T., Miguel, Y., Movshovitz, N., Kaspi, Y., Helled, R., Reese, D.,
1164 Galanti, E., Levin, S., Connerney, J. E. and Bolton, S. J., 2017. Comparing Jupiter interior structure models to Juno
1165 gravity measurements and the role of a dilute core. *Geophysical Research Letters*, 44, 4649–4659. 1707.01997
- 1166 Wang, D., Lunine, J. I. and Mousis, O., 2016. Modeling the disequilibrium species for Jupiter and Saturn: Implications
1167 for Juno and Saturn entry probe. *Icarus*, 276, 21–38. 1604.06371
- 1168 Wayne, R., 2000. *Chemistry of Atmospheres: An Introduction to the Chemistry of the Atmospheres of Earth, the*
1169 *Planets, and Their Satellites*. Oxford University Press
- 1170 Webster, C. R., Mahaffy, P. R., Atreya, S. K. et al, 2013. Low Upper Limit to Methane Abundance on Mars. *Science*,
1171 342, 355–357

1172 Webster, C. R., Mahaffy, P. R., Atreya, S. K. et al, 2015. Mars methane detection and variability at Gale crater.
1173 *Science*, 347, 415–417

1174 Webster, C. R., Mahaffy, P. R., Atreya, S. K., Moores, J. E., Flesch, G. J., Malespin, C., McKay, C. P., Martinez,
1175 G., Smith, C. L., Martin-Torres, J., Gomez-Elvira, J., Zorzano, M.-P., Wong, M. H., Trainer, M. G., Steele, A.,
1176 Archer, D., Sutter, B., Coll, P. J., Freissinet, C., Meslin, P.-Y., Gough, R. V., House, C. H., Pavlov, A., Eigenbrode,
1177 J. L., Glavin, D. P., Pearson, J. C., Keymeulen, D., Christensen, L. E., Schwenzer, S. P., Navarro-Gonzalez, R.,
1178 Pla-García, J., Rafkin, S. C. R., Vicente-Retortillo, Á., Kahanpää, H., Viudez-Moreiras, D., Smith, M. D., Harri,
1179 A.-M., Genzer, M., Hassler, D. M., Lemmon, M., Crisp, J., Sander, S. P., Zurek, R. W. and Vasavada, A. R., 2018.
1180 Background levels of methane in Mars' atmosphere show strong seasonal variations. *Science*, 360, 1093–1096

1181 Weidenschilling, S. J. and Lewis, J. S., 1973. Atmospheric and cloud structures of the jovian planets. *Icarus*, 20,
1182 465–476

1183 Wernicke, L. J. and Jakosky, B. M., 2021. Martian Hydrated Minerals: A Significant Water Sink. *Journal of Geo-*
1184 *physical Research (Planets)*, 126, e06351

1185 West, R. A., Baines, K. H., Friedson, A. J., Banfield, D., Ragent, B. and Taylor, F. W., 2007. Jovian clouds and
1186 haze. In *Jupiter. The Planet, Satellites and Magnetosphere* (F. Bagenal, T. E. Dowling, & W. B. McKinnon, eds.).
1187 Cambridge: Cambridge Univ. Press, 79–104

1188 West, R. A., Baines, K. H. and Pollack, J. B., 1991. *Clouds and aerosols in the Uranian atmosphere*. 296–324

1189 Whiteway, J. A., Komguem, L., Dickinson, C., Cook, C., Illnicki, M., Seabrook, J., Popovici, V., Duck, T. J., Davy,
1190 R., Taylor, P. A., Pathak, J., Fisher, D., Carswell, A. I., Daly, M., Hipkin, V., Zent, A. P., Hecht, M. H., Wood, S. E.,
1191 Tamppari, L. K., Renno, N., Moores, J. E., Lemmon, M. T., Daerden, F. and Smith, P. H., 2009. Mars Water-Ice
1192 Clouds and Precipitation. *Science*, 325, 68

1193 Wigner, E. and Huntington, H. B., 1935. On the Possibility of a Metallic Modification of Hydrogen. *Journal of*
1194 *Chemical Physics*, 3, 764–770

1195 Wildt, R., 1932. Absorptionsspektren und Atmosphären der grossen Planeten. *Veröffentlichungen der Universitaets-*
1196 *Sternwarte zu Goettingen*, 2, 171

1197 Wildt, R., 1940. Note on the Surface Temperature of Venus. *Astrophysical Journal*, 91, 266–268

1198 Winick, J. R. and Stewart, A. I. F., 1980. Photochemistry of SO₂ in Venus' upper cloud layers. *Journal of Geophysical*
1199 *Research*, 85, 7849–7860

1200 Wong, M. H., Mahaffy, P. R., Atreya, S. K., Niemann, H. B. and Owen, T. C., 2004. Updated *Galileo* probe mass
1201 spectrometer measurements of carbon, oxygen, nitrogen, and sulfur on Jupiter. *Icarus*, 171, 153–170

1202 Wurz, P., Rohner, U., Whitby, J. A., Kolb, C., Lammer, H., Dobnikar, P. and Martín-Fernández, J. A., 2007. The lunar
1203 exosphere: The sputtering contribution. *Icarus*, 191, 486–496

1204 Yelle, R. V. and Elliot, J. L., 1997. *Atmospheric Structure and Composition: Pluto and Charon*. 347

1205 Yelle, R. V. and McGrath, M. A., 1996. Ultraviolet Spectroscopy of the SL9 Impact Sites. *Icarus*, 119, 90–111

1206 Young, A. T., 1973. Are the Clouds of Venus Sulfuric Acid? *Icarus*, 18, 564–582

- 1207 Yung, Y. L. and Demore, W. B., 1982. Photochemistry of the stratosphere of Venus: Implications for atmospheric
1208 evolution. *Icarus*, 51, 199–247
- 1209 Yung, Y. L. and DeMore, W. B., 1999. *Photochemistry of Planetary Atmospheres*. New York: Oxford Univ. Press
- 1210 Zahnle, K., Freedman, R. S. and Catling, D. C., 2011. Is there methane on Mars? *Icarus*, 212, 493–503
- 1211 Zalucha, A. M. and Cook, J., 2019. *The Structure and Dynamics of the Atmospheres of Pluto and Triton*. 113
- 1212 Zhang, J., Dauphas, N., Davis, A. M., Leya, I. and Fedkin, A., 2012. The proto-Earth as a significant source of lunar
1213 material. *Nature Geoscience*, 5, 251–255
- 1214 Zolotov, M., 2019. Chemical Weathering on Venus. *Oxford Research Encyclopedia of Planetary Science*, 146
- 1215 Zolotov, M. Y., 2018. Gas-Solid Interactions on Venus and Other Solar System Bodies. *Reviews in Mineralogy and*
1216 *Geochemistry*, 84, 351–392